A Novel Hybrid of Chloroquine and Primaquine Linked by Gold(I): Multitarget and Multiphase Antiplasmodial Agent

Caroline de Souza Pereira,[a] Helenita Costa Quadros,[b] Diogo Rodrigo Magalhaes Moreira,[b] William Castro,[c] Romulo Ivisson Santos De Deus Da Silva,[b] Milena Botelho Pereira Soares,[b] Diana Fontinha,[d] Miguel Prudêncio,[d] Vinicius Schmitz,[a] Hélio F. Dos Santos,[a] Mathieu Gendrot,[e, f, g] Isabelle Fonta,[e, f, g, h] Joel Mosnier,[e, f, g, h] Bruno Pradines,[e, f, g, h] and Maribel Navarro*[a]

Plasmodium parasites kill 435 000 people around the world every year due to unavailable vaccines, a limited arsenal of antimalarial drugs, delayed treatment, and the reduced clinical effectiveness of current practices caused by drug resistance. Therefore, there is an urgent need to discover and develop new antiplasmodial candidates. In this work, we present a novel strategy to develop a multitarget metallic hybrid antimalarial agent with possible dual efficacy in both sexual and asexual erythrocytic stages. A hybrid of antimalarial drugs (chloroquine and primaquine) linked by gold(I) was synthesized and characterized by spectroscopic and analytical techniques. The CQPQ-gold(I) hybrid molecule affects essential parasite targets, it inhibits β-hematin formation and interacts moderately with the DNA minor groove. Its interaction with PfTrxR was also examined in computational modeling studies. The CQPQ-gold(I) hybrid displayed an excellent *in vitro* antimalarial activity against the blood-stage of *Plasmodium falciparum* and liver-stage of *Plasmodium berghei* and efficacy *in vivo* against *P. berghei*, thereby demonstrating its multiple-stage antiplasmodial activity. This metallic hybrid is a promising chemotherapeutic agent that could act in the treatment, prevention, and transmission of malaria.

Introduction

Over a long period of time, a number of complementary strategies were employed to control malaria. The World Health Organization highlighted that the most advanced malaria vaccine candidate shows only partial protection against malaria in young children. It also called attention to insecticide-treated net as well as indoor residual spraying as powerful ways to immediately reduce malaria transmission. Regarding the chemotherapy strategy, the best available treatment for *Plasmodium falciparum* malaria is artemisinin-based combination therapy (ACT) using two or three well-known antimalarial drugs. Despite all the enormous efforts, malaria is still an important health problem, where in 2018, 228 million cases of malaria and 405 000 deaths around the world were reported.[1]

Malaria treatment with a cocktail of drugs or combination of drugs is showing critical limitations, such as poor patient compliance and a high risk of drug-drug interactions.[2] Further complications are reports of increased resistance to ACT.[3] Among many different approaches to antimalarial drug discovery and development, the antimalarial organic hybrid molecules must be cited. A plethora of examples of these kind of compounds have been studied so far.[4–6] A hybrid compound is defined as a chemical entity with two or more structural domains which acts on different or same biological function or with dual mode of action.[2] The most classic examples are trioxaquine,[7] trioxaferroquines[7] and primaquine/chloroquine hybrid.[5] The advantages of organic hybrid compounds are the possibility of additive or synergistic therapeutic response, improved druggable characteristics of the therapeutic compo-

[a] C. de Souza Pereira, V. Schmitz, Prof. H. F. Dos Santos, Prof. M. Navarro
Departamento de Química
Universidade Federal de Juiz de Fora, Rua José Lourenço Kelmer, s/n – Campus Universitário, Bairro Martelos CEP 36036-900, Juiz de Fora, Minas Gerais (Brasil)
E-mail: maribel.navarro@ufjf.edu.br
[b] H. Costa Quadros, Dr. D. R. Magalhaes Moreira,
R. I. Santos De Deus Da Silva, Dr. M. Botelho Pereira Soares
Instituto Gonçalo Moniz
Fundação Oswaldo Cruz, Av. Waldemar Falcão, 121, Candeal, Salvador, Bahia (Brasil)
[c] Dr. W. Castro
Centro de Química
Instituto Venezolano de Investigaciones Científicas (IVIC), Centro de Química, Carretera Panamericana, Km 11, Altos de Pipe, San Antonio de los Altos Miranda, 1020-A, Caracas (Venezuela)
[d] Dr. D. Fontinha, Dr. M. Prudêncio
Instituto de Medicina Molecular João Lobo Antunes
Faculdade de Medicina, Universidade de Lisboa
< Lisboa (Portugal)
[e] M. Gendrot, I. Fonta, J. Mosnier, Dr. B. Pradines
Unité Parasitologie et entomologie, Institut de recherche biomédicale des armées, 19–21 Bd Jean Moulin, 13005 Marseille (France)
[f] M. Gendrot, I. Fonta, J. Mosnier, Dr. B. Pradines
Aix-Marseille Univ, IRD, SSA, AP-HM, VITROME, 19–21 Bd Jean Moulin, 13005 Marseille (France)
[g] M. Gendrot, I. Fonta, J. Mosnier, Dr. B. Pradines
IHU Méditerranée Infection, 19–21 Bd Jean Moulin, 13005 Marseille (France)
[h] I. Fonta, J. Mosnier, Dr. B. Pradines
Centre National de Référence du Paludisme, 19–21 Bd Jean Moulin, 13005 Marseille (France)

Supporting information for this article is available on the WWW under https://doi.org/10.1002/cmdc.202000653

This article belongs to the joint Special Collection with the European Journal of Inorganic Chemistry, "Metals in Medicine" and also to the Special Collection "BrazMedChem 2019: Medicinal Chemistry in Latin America".

nent and prolonged antiparasitic duration.[2] A potential limitation for the two covalently linked antimalarial drug moieties is to reach localized targets. This, especially inside of digestive vacuole of the malarial parasite, can be a challenge.

A valuable approach is to connect two or more existing and well-known clinical antimalarial drugs with a transition metal to form a single chemical entity, named as metallic hybrids. It might be obvious to start designing this antimalarial metallic hybrid with the most successful antimalarial drug, chloroquine (CQ; Figure 1). Despite CQ-resistant (CQR) malaria parasites had spread worldwide, CQ is a potent hemozoin inhibitor,[8] and that reflects its remarkable accumulation inside digestive vacuole.[9] By inhibiting the formation of hemozoin[10] CQ kills the malarial parasites and acts in the intra-erythrocytic stage of the asexual *P. falciparum* life cycle.[11]

Another antimalarial drug for such metallic hybrid compound can be primaquine (PQ; Figure 1), This is one of few, commercially available gametocidal drugs, which acts in the sexual cycle of *P. falciparum* and blocks the transmission of the disease.[12] In addition, PQ has antiparasitic activity against the liver stage that is important for controlling the disease. As a limitation, PQ is extensive metabolized into approximately five major metabolites, where the concentration and composition vary according to different population, limiting PQ efficacy for transmission and controlling malaria.[13]

Gold(I)-based compounds, such as auranofin[14] and gold(I)-chloroquine complexes[15–17] have shown excellent antimalarial activity against *P. falciparum*, even against CQ-resistant strains. Recently, it was demonstrated that gold(I)-phosphine complexes were able to attenuate the viability of parasites,[18] reinforcing the potential of gold as a transition metal in antiparasitic therapy. Gold(I) compounds mainly act as inhibitors of the thioredoxin reductase (TrxR) system, which is present in parasites and also in cancer cells.[19,20] According to molecular modeling techniques gold(I) compounds can be capable to inhibit the *P. falciparum* thioredoxin reductase (PfTrxR),[21] which is an essential enzyme for the survival of this parasite.[22] Hence, a novel hybrid compound consisting of these two, well-known antimalarial drugs connected by gold atom has been developed in this work that fits with the 'master key' compounds and can favorably interact with multiple parasite targets.[23] Additionally, it was envisaged that this rational design would produce a multiple-stage antiparasitic agent which can be successful in the treatment, prevention and transmission of malaria.

Accordingly, the synthesis and characterization of this multitarget metal-antimalarial drugs hybrid, with possible dual efficacy in the sexual and asexual plasmodial stages. The mechanisms of action of our metallic hybrid molecule were evaluated through its interactions with three essential parasite targets: DNA (reversible and/or covalent interactions), heme (interaction with FPIX and inhibition of β-hematin formation), and PfTrxR using computational modelling studies. Importantly, antimalarial activity was estimated using both *in vitro* and *in vivo* models.

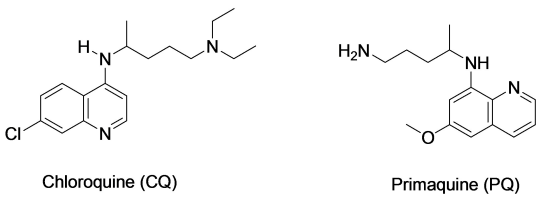

Figure 1. Structure of antimalarial drugs.

Results and Discussion

Synthesis and characterization of the hybrid gold(I) linker antimalarial drugs

The development of the hybrid of clinical antimalarial drugs linked by gold was inspired by the great antimalarial activity *in vitro* and *in vivo* of $[AuCQPPh_3]PF_6$ complex, which also acts at least in three distinct parasites targets (hemozoin, thioredoxin reductase and DNA) as we reported previously.[17,24,25] In view of that, we designed a gold(I) hybrid that contains not only chloroquine, but also primaquine, in order to investigate its potential to act as multitarget and be used against both sexual and asexual erythrocyte stages (dual phases) in the malarial parasite. This gold(I)-antimalarial drugs hybrid was obtained in a two-step reaction (Scheme 1). The first step consisted of the replacement of tetrahydrothiophene (THT) in the coordination sphere of Au(THT)Cl complex by primaquine that led to the AuPQCl intermediate. In the second step, this intermediate was dissolved in acetonitrile and mixed with an excess of NH_4PF_6 at room temperature to replace the chloride ligand, and the subsequent rapid coordination of chloroquine at low temperature which resulted in the hybrid $[AuCQPQ]PF_6$. It was isolated as brown solid. The stability of $[AuCQPQ]PF_6$, also known as CQPQ-gold(I) hybrid was evaluated in DMSO by ^1H and ^{31}P NMR

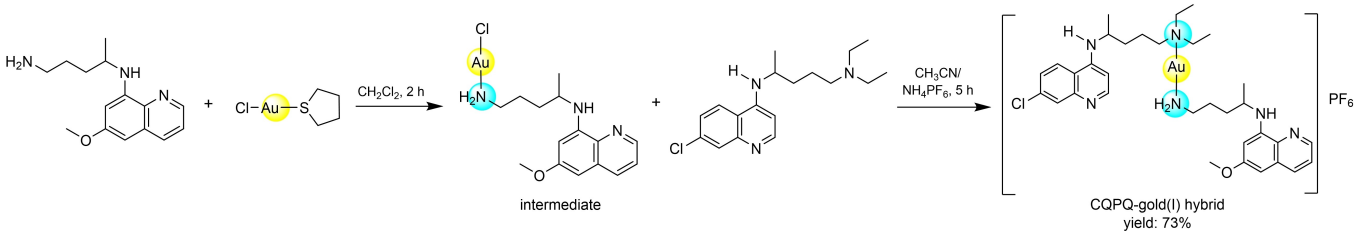

Scheme 1. Synthesis of $[AuCQPQ]PF_6$ hybrid.

studies after 31 days, in the interim, its stability in propylene glycol and in culture medium was followed by UV-visible, no changes were observed and this indicated that the hybrid [AuCQPQ]PF_6 molecule is stable in these solutions, which are also used in the biological tests (Figures S1–S4 in the Supporting information).

The CQPQ-gold(I) hybrid was characterized using several analytical and spectroscopic techniques. The IR spectrum showed the characteristic and relevant bands of the ligands CQ and PQ slightly displaced when compared to the same bands of the free ligands. The presence of others important bands at 557 and 844 cm^{-1} correspond to νAu–N[26] and the counter ion νPF_6, respectively (Figure S5). Similarly, the UV/Vis absorption spectrum displayed the peaks associated with both ligands CQ and PQ slightly shifted (Figure S6). The results obtained from the elemental analyses and molar conductivity studies in DMSO confirmed the molecular formula proposed and that this compound is an electrolyte substance 1:1. The MALDI mass spectrum of metallic hybrid showed some important peaks attributed to the molecular fragment of $[Au\text{-}PQ]^+$ (456.14 *m/z*), and the corresponding peak of the free CQ at 320 m/z. Peak for the molecular ion was not observed (Figure S7).

One- and two-dimensional NMR spectra provided essential information for the full elucidation of the molecular structure of CQPQ-gold(I) hybrid, as described in our previous papers[25] and also reported by other investigation groups.[27,28] The variation in the ^1H and ^{31}C chemical shifts of each signal in the metal complex compared to those of the free ligands ($\Delta\delta$) can be used to deduce information about the coordination mode of the ligands to the metal. Both ligands, PQ and CQ, contain several, distinct donor nitrogen atoms that are able to coordinate to the gold ion. The coordination site is indicated by the largest variation in the ^1H and ^{31}C chemical shifts in the vicinity of these N atoms. The comparative analysis of the ^1H NMR spectra of the free ligands (CQ and PQ) and that of the gold(I)-antimalarial drugs hybrid (Figure S8) showed displacements of protons Hd′ ($\Delta\delta = 0.22$), H4′,5′ (0.43), H6′ (0.16) in the CQPQ-gold(I) hybrid, while the rest of the protons were not affected. These results suggest the coordination of PQ to gold through the primary amine NH_2, and that of CQ through the tertiary amine. The integration of each signal of ^1H NMR spectrum of CQPQ-gold(I) hybrid confirmed that its composition and that only one molecule of each antimalarial drug coordinated to gold(I) ion (Figure S9).

In the ^{13}C NMR spectrum of CQPQ-gold(I) hybrid (Figure S10) was observed all the carbon signals correspond to each carbon of the ligands (PQ and CQ), it was also noticed that C6′ ($\Delta\delta = 1.85$ ppm), Cb′ ($\Delta\delta = 1.28$ ppm), Cc′ ($\Delta\delta = 6.37$ ppm) and Cd′ ($\Delta\delta = 2.66$ ppm) were significantly shifted. This is consistent with ^1H NMR results, namely that the PQ and CQ coordination to gold occurred trough the nitrogen (N**3** for CQ and N**c** for PQ) atoms. CQ coordination to gold through N**3** was already described for Au^{III}–CQ complex.[15] In the ^{31}P NMR (Figure S11) a septuplet at −144 ppm was observed, confirming the presence of the counter ion PF_6^-.

^1H,^{15}N gHMBC correlations (Figures S12–S14) were performed in order to provide additional structural data and to unequivocally establish the coordination of each ligand (PQ and CQ) to gold ion via the nitrogen atoms. Table 1 shows the chemical shifts of each signal for PQ, CQ and CQPQ-gold(I) hybrid which confirm that CQ binds to the gold ion by N**3** atom, corroborating the coordination mode described above. The values obtained are also in good agreement with the literature.[29]

The results discussed above suggest that the CQPQ-gold(I) hybrid, consisting of the gold linked the antimalarial drugs primaquine (gametocytocidal agent) and chloroquine (schizonticidal agent), which is a cationic metal complex with linear geometry and hybridization sp.

The density functional theory (DFT)-optimized structure of the CQPQ-gold(I) hybrid (Figure 2) shows two conformers. Structure **A** was found slightly more stable than **B** by only 3.1 kJ mol^{-1}, suggesting that both forms could coexist in a polar solvent. Of note, such ligand flexibility might be a favorable factor for a multitarget agent.

The ^1H and ^{13}C NMR chemical shifts were calculated for CQ and PQ ligands and for the CQPQ-gold(I) hybrid structure **A**. In the CQ ligand, low field shifts are predicted for H3′ ($\Delta\delta = 0.41$ ppm), H4′,5′ ($\Delta\delta = 0.39$ ppm) and H6′ ($\Delta\delta = 0.17$ ppm) and similarly, in the PQ ligand for Hc′ ($\Delta\delta = 0.19$ ppm) and Hd′ ($\Delta\delta = 0.09$ ppm). Concerning the ^{13}C NMR, low field shifts are predicted for C4′ ($\Delta\delta = 4.76$ ppm), C5′ ($\Delta\delta = 4.56$ ppm), C6′ ($\Delta\delta = 1.47$ ppm) in the CQ side, and in the PQ side for Cd′ ($\Delta\delta = 2.18$ ppm) and a high field shift for Cc′($\Delta\delta = -1.78$ ppm) and Cb′ ($\Delta\delta = -2.43$ ppm). These two latter results are distinct from experimental results, which suggest pronounced low field shifts for Cb′, Cc′ and Cd′ nuclei. The reason for such discrepancy between the experimental and calculated values has not been fully understood. One would not expect an error larger than 5% for ^{13}C calculated chemical shift, especially, when relative values are concerned. One possible reason for this is that the solvation model does not account for specific

Table 1. ^{15}N RMN chemical shifts (δ) for the free ligands (PQ and CQ) and the [AuCQPQ]PF_6 hybrid in [D_6]DMSO.

CQ δ (ppm)	PQ δ (ppm)	[AuCQPQ]PF_6 hybrid (ppm)	$\Delta\delta$ (ppm)
N**1** 268.02	N**a** 295.26	N**1** 265.16	2.86
N**2** 94.08	N**b** 81.82	N**2** 93.94	0.14
N**3** 43.68	N**c** –	N**3** 52.35	**8.67**
		N**a** 295.27	0.01
		N**b** 80.53	1.29
		N**c** –	–

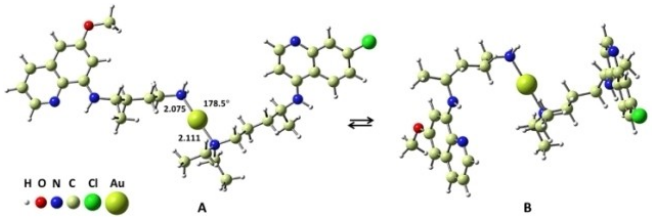

Figure 2. DFT-optimized structure of the CQPQ-gold(I) hybrid. Two distinct conformations are shown, with form **A** being 3.1 kJ mol^{-1} more stable than **B**. The Au–N bond length is given in Å and the N–Au–N angle in degrees.

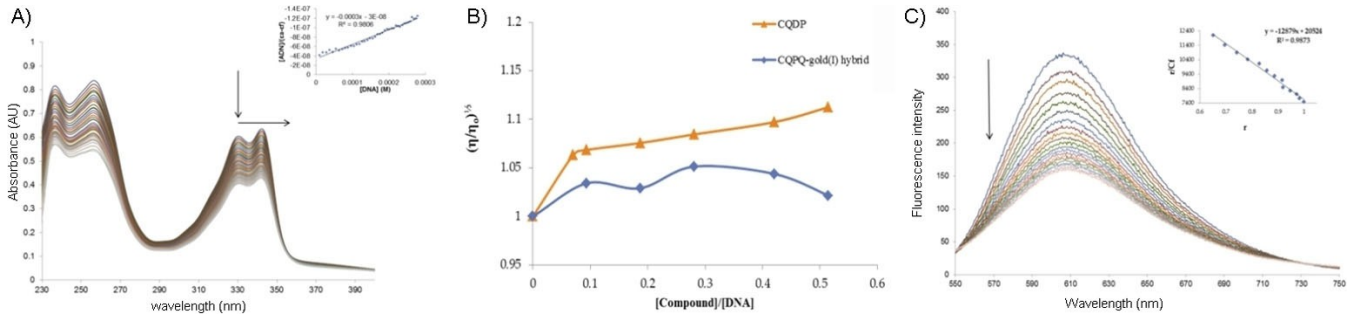

Figure 3. Interaction studies of [AuCQPQ]PF_6 with CT-DNA. A) Spectrophotometric titrations. B) Viscosity studies. C) Competitive DNA-binding studies.

solute-solvent interactions. Despite this disagreement with the experimental results, most of the relative chemical shifts from the theoretical NMR signals suggest complex structure **A** in alignment with the experimental interpretation of the proposed coordination mode as represented in Figure 2. The Figure S15 compares the calculated and experimental chemical shifts for all H and C atoms in the CQPQ-gold(I) hybrid structure. The average absolute errors were 7.4 ppm for ^{13}C and only 0.56 ppm for ^{1}H, corresponding to an overall relative error of only 11%.

Gold(I) linker antimalarial drugs hybrid as a multitarget drug

Interaction studies of [AuCQPQ]PF_6 with DNA

Reversible interactions between [AuCQPQ]PF_6 with the DNA helix have been studied through the classical spectrophotometric titrations.[30–32] The results are displayed in Figure 3A, the hybrid [AuCQPQ]PF_6 exhibits two intense absorption bands in the range 200–270 nm and 310–370 nm which is attributed to n→π* and π→π* transition absorptions, respectively. The increased amount of DNA added to a solution of CQPQ-gold(I) hybrid until saturation caused hypochromism in both bands. The band maximums at 257 and 343 nm showed a significant decreased in the absorbance (32.8 and 34.4% respectively) and slight blue shift of 2 nm. These results are comparable to those observed with other compounds with known interactions with DNA, such as ethidium bromide (EB; Table 2) and with other metal complexes with antimalarial activity.[33] The binding constants (K_b) obtained for CQPQ-gold(I) hybrid, CQDP (chloroquine diphosphate) and EB are shown in Table 2. The K_b value of our antimalarial gold(I) hybrid is similar than those listed or those previously reported for antitumor metal complexes.[34–36]

Table 2. Data obtained from different spectroscopic and analytical methods for DNA interaction with compounds.

Property	EB	CQDP	[AuCQPQ]PF_6
absorbance[a] (±1 nm)	286	340	342
hypochromism[a] (±0.2%)	67.1%	19.5%	37.5%
K_b x 10^4 (M^{-1})[a]	1.33±0.02	10.19±0.15	1.19±0.02
K_b x 10^5 (M^{-1})[b]	–	3.11±0.29	0.12±0.01

[a] Absorbance measurements. [b] Fluorescence measurements.

The constant is in the same range as that of the similar compound [Au(CQ)(PPh_3)]PF_6 reported by us, that shows an antimalarial activity superior to the CQDP (chloroquine diphosphate) specifically in resistant strains,[24] the values of the constant are in the same range. Given all these results, some reversible interactions, such π–π stacking, and interaction dipole or hydrogen bridging appear to be taking place.

Additional information to explore the CQPQ-gold(I) hybrid-DNA interactions was collected from the viscosity measurements; these studies were performed using an Osward viscometer. The hydrodynamic behavior of DNA, specifically in the presence of small molecules (metallodrug) in different ratios [compound]/[DNA], can be examined through the changes in the viscosity of DNA, which is associated with the modes of binding. This can be distinguished effectively, as covalent and noncovalent binding modes display different hydrodynamic characteristics. Noncovalent interaction such as intercalators induce extension and unwinding of the DNA backbone, while for noncovalent major and minor groove binding compounds cause little or no distortion to the DNA.[37] The results for CQDP and CQPQ-gold(I) hybrid with DNA are shown in Figure 3B. Chloroquine increased the relative viscosities of DNA, acting predominantly as intercalate compound,[25,38] what was already expected, once free CQ intercalates into DNA.[38] CQPQ-gold(I) hybrid slightly increased the relative viscosity of the DNA at lower [compound]/[DNA] ratio, but at higher ratio only small variations of the relative viscosity of DNA were observed. The analyses of this data suggest that our metallic hybrid can interact with the DNA by reversible binding, and it can interact by intercalation or minor groove interaction with DNA. The mode of binding could be concentration dependent.[39]

In view of the results of the viscosity studies, the effect of interaction between the [AuCQPQ]PF_6 hybrid and DNA was also investigated using ethidium bromide as a fluorescence probe. EB emits intense fluorescence in the presence of DNA because of the strong interaction between the adjacent base pairs of DNA ($K_b = 1.4 \times 10^6$ M^{-1}).[40] The [AuCQPQ]PF_6 does not show any significant fluorescence at room temperature in the presence or absence of CT DNA, when excited at 471 nm. Furthermore, the addition of the CQPQ-gold(I) hybrid to a solution containing EB alone does not provoke quenching of free EB fluorescence and appearance of any new peak in the spectra. Therefore, any changes observed in the fluorescence emission spectra of a

solution containing the EB-DNA system at 471 nm when adding the metallic hybrid is because of the ability of the compound to interfere with the EB-DNA system. The addition of $[AuCQPQ]PF_6$ at different Cb/[DNA] ratio to the EB-DNA system, decreases the intensity of the emission band at 607 nm (Figure 3C). This demonstrates the moderate interaction of the compound with the EB-DNA system, possibly due to the displacement of EB resulting in fluorescence quenching.

According to the Scatchard equation,[41] a plot of r/C_f versus r gave K_b values of $(0.12 \pm 0.05) \times 10^5$ and $(3.11 \pm 0.09) \times 10^5\ M^{-1}$ from the fluorescence data for the CQPQ-gold(I) hybrid and CQDP respectively, showing a possible displacement of EB similar to other metal complexes with reported biological activity.[42–44] This displacement can indicate intercalation or minor groove interaction.[45–48] The results also show that the DNA-binding affinity of CQPQ-gold(I) hybrid is mild, which agrees with the results obtained from electronic absorption spectra and viscosity measurements.

We also evaluated this interaction with the DNA by gel-electrophoresis, where the presence of interaction is determined through the variation of the electrophoretic mobility of the DNA. The pBR322 plasmid, is a supercoiled (SC) DNA, but it can be converted into open circular (OC) or linear (L) when in contact with some harmful agents. SC is the form that migrates faster, L is intermediate and OC is the one with greater difficulty to migrate in the agarose gel.[37] The effect of the interaction of CQPQ-gold(I) hybrid with the DNA plasmid on the variations of the electrophoretic mobility of the DNA plasmid was examined. The results obtained from this experiment (Figure S16) revealed no significant changes in the electrophoretic mobility between that of the free plasmid pBR322 and that with incubated with CQPQ-gold(I) hybrid for 17 h. The hybrid ($[AuCQPQ]PF_6$) does not cleave the DNA supercoil and does not alter the tertiary structure of the DNA under these conditions, suggesting that the CQPQ-gold(I) hybrid interacts with the DNA in a non-covalent manner, in the same way shown for metal-chloroquine complexes.[24,38]

The *in silico* analysis showed that the CQPQ-gold(I) hybrid binds to the minor groove of the DNA (Figure S17). The ligands do not intercalate between the base pairs, but instead the CQ moiety is hydrogen bonded to a phosphate group with distance of 1.82 Å, and the PQ ligand is twisted out from the minor groove. The binding energy (ΔE_b) calculated over 500 frames from MD trajectory was -94.4 ± 0.3 kcal mol^{-1}, ~85% due to electrostatic interaction and ~15% from van der Waals contributions. It is noted in Figure S17D that the DNA structure maintains its structure close to the solid state with an average root mean square deviation (RMSD) of only 1.98 Å. This is a consequence of the weak ligand-DNA interaction, in agreement with the experimental findings.

Collectively, our results suggest that our CQPQ-gold(I) hybrid binds the DNA primarily through noncovalent interactions through moderate electrostatic contacts at the minor groove region and π–π stacking interactions between them could also happen. Once the interaction of our metallic hybrid was evaluated with the DNA, one of the important parasite targets, we went further to validate our rational design of $[AuCQPQ]PF_6$ being a multitarget drug. The second identified essential target (inhibition of β-hematin formation) for malarial parasite was evaluated and the results are shown in the following section.

Heme as an important target for $[AuCQPQ]PF_6$

Malaria parasites digest hemoglobin for their growth and to replicate, however in this process heme is accumulated which is toxic to the parasite. To avoid death, the parasite converts heme into the insoluble and inert hemozoin crystals in its digestive vacuole. This vital process for the parasite survival stands out as a selective target to be attacked by the antimalarial drug, in fact, this is the most accepted mechanism of action of chloroquine.[10]

CQ have been shown to form adducts with $Fe^{III}PPIX$[16] and consequently inhibiting the hemozoin formation. Converting $Fe^{III}PPIX$ is a target for anti-malarial drugs. Therefore, the interaction of CQPQ-gold(I) hybrid with ferriprotoporphyrin was first evaluated by UV/Vis spectroscopic titration to determine the association constant ($\log K$) of the compound with $Fe^{III}PPIX$, and also to monitor the presence of perturbations in the Soret's band of porphyrin (402 nm) with increasing concentration of the CQPQ-gold(I) hybrid. The observed $\log K$ for the CQPQ-gold (I) hybrid (Table 3) was similar to CQ. The increasing concentration of the metallic hybrid also caused a hypochromism of 65% (Figure 4). This result indicates that the CQPQ-gold(I) hybrid interacts with ferriprotoporphyrin similarly to CQ and metal-CQ complexes under same experimental condictions.[16] As the CQPQ-gold(I) hybrid interacts with ferriprotoporphyrin, it might have the ability to inhibit the β-hematin formation, therefore we evaluated the capacity of the hybrid to inhibit β-hematin formation.

Synthetic β-hematin is identical to hemozoin (malaria pigment).[49] The inhibition of β-hematin formation by a simple and cheap technique such as the Infrared spectroscopy, has

Table 3. Interaction with hemin, inhibition of β-hematin formation and lipophilicity studies.

	Interaction with hemin	Inhibition of β-hematin formation			Lipophilicity studies	
Compound	$\log K$ [a]	IR	HAI_{50} (mM) in buffer[c]	HAI_{50} (mM) at interface[d]	$\log D$ (pH 5.1)	$\log D$ (pH 6.9)
0.14 ± 0.06 (1,3)	0.71 ± 0.08 (4)	+			−2.0	0.98
CQ	4.99 ± 0.01	+	0.11 ± 0.03 (1)	2.82 ± 0.09 (1)	−1.53	0.38
PQ	n.d.[b]	−			−0.41	2.0

HAI_{50} is the drug-to-hemin ratio required to inhibit 50% of heme aggregation against a control experiment in the absence of drugs. [a] pH ~ 5. [b] Not detectable. [c] After 24 h of reaction. [d] After 2 h of reaction. Values in parentheses are the relative activity with respect to CQDP.

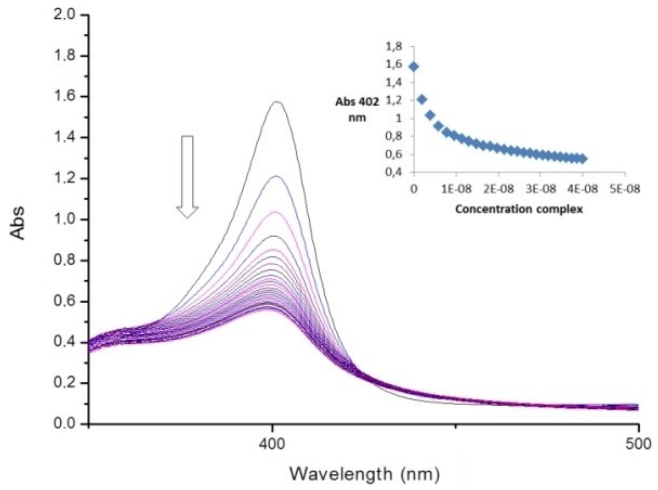

Figure 4. Spectroscopic titration of ferriprotoporphyrin with the CQPQ-gold (I) hybrid. Conditions: 40% DMSO, pH 7.5 and [CQPQ-gold(I) hybrid] = 0.02 mM.

been well documented by Egan et al.,[50] thus, this method was utilized in the present work for evaluating if our [AuCQPQ]PF_6 is able to inhibit β-hematin formation.

β-Hematin is a dimer of Fe^{III}PPIX, where the ionized heme-propionate side chain of one Fe^{III}PPIX coordinates to the Fe of the other, characterized by two bands in the infrared spectrum: 1663 cm^{-1} from C═O and 1210 cm^{-1} from C–O stretch of carboxylate group coordinated to the Fe^{III} center.[51] Knowing that CQ inhibits the hemozoin formation, we first investigated the qualitative inhibition of β-hematin formation by our metallic hybrid in solid state, using FTIR spectroscopy to characterize the reaction products. The resulting IR spectrum (Figure 5) shows no IR bands corresponding to C═O and C–O stretch, while these bands are present for primaquine (negative control) and absent for CQ (control positive) indicating that our metallic hybrid inhibits β-hematin formation in a similar manner to CQ.[50]

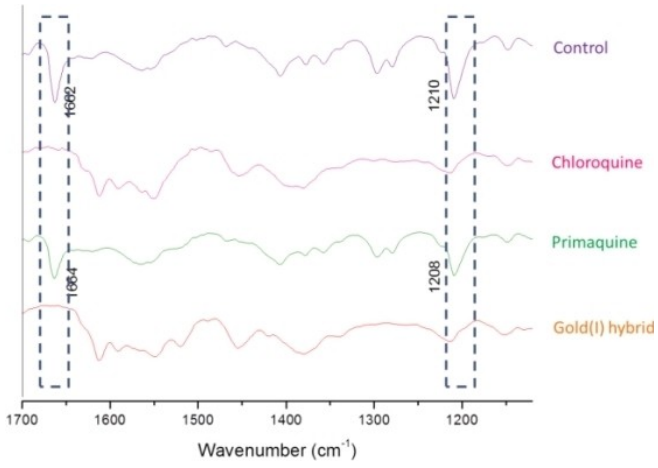

Figure 5. FTIR spectroscopic characterization of the inhibition of β-hematin formation by chloroquine, primaquine, CQPQ-gold(I) hybrid and the control.

In order to obtain quantitative data for the heme aggregation inhibition activity (HAIA) of [AuCQPQ]PF_6, a set of experiments were performed in acetate buffer and also at the interface of *n*-octanol/aqueous buffer; the results were then compared to those for CQDP as control. The IC_{50} value measured for CQPQ-gold(I) hybrid in acetate buffer at pH 5 indicates that the metallic hybrid is able to inhibit the heme aggregation process and displays an activity very similar to that of CQDP in these conditions.

Subsequently in another experiment with more realistic conditions using the interfaces of *n*-octanol/water where the β-hematin assembles rapidly and spontaneously, following an adaptation of the procedure described by Egan et al.[52] and also reported by Sánchez-Delgado et al..[53] At this interface, the [AuCQPQ]PF_6 is significantly more potent than CQDP for inhibiting heme aggregation near the interface, more interesting, this result is similar to [Au(CQ)(PPh_3)]PF_6, reported by us.[24] These results suggest that the CQPQ-gold(I) hybrid shows antiplasmodial activity similar to CQDP in sensitive strains, while in resistant strains enhanced activity, to avoid resistance, as was observed for other metal-CQ complexes with antimalarial activity, for example [$RuCl_2$(CQ)]$_2$,[32] [Au(CQ)(PPh_3)]PF_6[24] or Au(CQ)(Cl).[16]

In silico study of interaction of CQPQ-gold(I) hybrid with P. falciparum *thioredoxin reductase (PfTrxR) enzyme*

Molecular modeling techniques were applied to gain some molecular insights on the [AuCQPQ]PF_6–PfTrxR binding mode. The first approach was to perform a docking study in order to select representative poses for ligand-enzyme complex (see Figure S18 and the related discussion). Docking results are semi-quantitative only and more accurate potential need to be used to expand and quantify the analysis. This was done by MD simulation, in which the ligand-enzyme structures obtained from the docking study were used as starting point for MD simulation.

There are two equivalent binding sites in the enzyme, but just one ligand was considered as docked at the site formed by the C-terminal of monomer **2** and N-terminal of monomer **1**. Overall, the structure of the enzyme does not change significantly due to the ligand binding, as shown by the RMSD values along the MD trajectory in Figure S19A. When the root mean square fluctuation (RMSF) data are compared in Figure S19B we noted that the enzyme structure becomes more rigid (lower values of RMSF) in the ligand-enzyme complex in Pose 1 and 2 and more flexible in Pose 3 (higher values of RMSF). For the last Cys in the C-terminal motif (Cys540 in the original PDB numbering or Cys1007 in the current numbering scheme), the RMSF drops from 6.36 Å (free protein) to ~3 Å (Poses 1 and 2) and to 4.9 Å (Pose 3). An important parameter in these poses is the S(Cys540)–Au distance, which must be short enough to allow the approach of Cys540 by the metal center. The distance varies along the MD trajectory and the average values are (in Å): 11 ± 1 (Pose 1), 7.5 ± 0.7 (Pose 2) and 6.0 ± 0.9 Å (Pose 3). These results suggest that the CQPQ-gold(I) hybrid and S(Cys)

in Poses 2 and 3 are close enough to bind, and this state could be viewed as a pre-reactive arrangement, representing the Michaelis-Menten type complex.[54]

The [AuCQPQ]PF_6–PfTrxR binding modes are visualized in the snapshots of Figure 6 (Pose 2 – the most stable) and Figure S20 (Poses 1 and 3).

Only one frame is represented in Figure 6 and S20, which does not totally reflect the ligand-enzyme average contact throughout the entire MD trajectory, however, some important residues, which are in close contacts with the ligand, are highlighted and labeled. In Figure S21 A–C the total number of contacts calculated along the MD trajectory is plotted for every residue in the protein. Pose 1 (Figure S20 A, C) is found deep inside the binding site (close to the N-terminal motif). Pose 2 (Figure 6) and Pose 3 (Figure S20 B, D) are similar to each other, with contacts preserved in the α-helix including Phe106 and Ser103. Pose 2 (Figure 6) also showed some significant interactions between the ligand and Asp897 (weak H-bond = 2.47 Å) and Lys999 (weak H-bond = 2.35 Å) residues. Unlike in Pose 1, in Poses 2 and 3, the C-terminal cysteines are close to the ligand

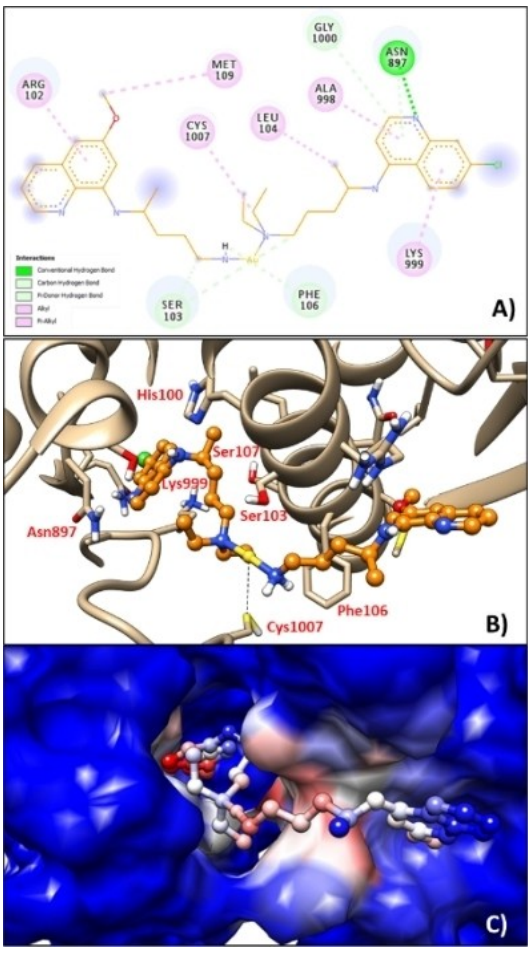

Figure 6. Binding mode of the CQPQ-gold(I) hybrid and PfTrxR enzyme obtained from MD simulation in aqueous solution (Pose 2). A) 2D diagram representing the main residues in contact with the ligand. B) 3D structure of the drug-receptor complex. C) Enzyme van der Waals surface with colors representing the frequency of drug-receptor contacts (scale: red: 60, white: 30, and blue: 0).

and these contacts are frequent in the MD trajectory (Figure S21 B, C).

The binding energy was calculated from MD trajectory using the MMGBSA approach where 250 frames evenly spaced in time. The values are given in Table S1 which includes the overall binding energy and the individual contributions. Using a more accurate approach, Pose 2 was predicted as the most stable among those tested, followed by Pose 3. The Pose 1 was the least stable according to the MMGBSA. The values in Table S1 show that the VDW energy contribution is dominant and drives all binding processes, being more pronounced for the most extended ligand forms, which have a large contact surface with the enzyme. Summing up, the MD predicted the Pose 2 (Figure 6) as the most favorable binding mode, being the ligand-enzyme interaction driven mainly by the van der Waals contribution. Moreover, in Pose 2 the Cys540 at the C-terminal was at 7.5 Å on average apart from the Au center suggesting a pre-reactive arrangement necessary for enzyme inhibition. Our molecular modeling predicted that CQPQ-gold(I) hybrid complex can bind to the PfTrxR enzyme at the C-terminal motif where the ligand assumes an extended conformation with the Au center close to the Cys540. This arrangement is represented by Pose 2 (Figure 6) and might be viewed as the Michaelis-Menten complex prior the ligand exchange reaction. A detailed view of Pose 2 binding mode is represented in Figure 6C where we see the CQ moiety inside the binding site (in red) and the PQ ligand outside the interface tunnel (in blue). This suggests a primary role of CQ ligand to bind effectively to PfTrxR, which is an important finding to design new and potent hybrid complexes as inhibitors of PfTrxR.

Lipophilicity studies

Table 3 shows the distribution coefficients (log *D*) for the CQPQ-gold(I) hybrid at pH 5 and 6.9, calculated by log *D* = log [compound in *n*-octanol]/[compound in water]. Log *D* < 0 suggest that the compound is more hydrophilic, log *D* > 0 more lipophilic and log *D* = 0 that it has the same affinity for both phases.[55] Based on the log *D* values obtained for [AuCQPQ]PF_6, it is noticeable that this compound presents similar behavior to CQ, that is, it is more hydrophilic at pH 5.1 and more lipophilic at pH 6.9. This fact indicates that at the pH of the malarial parasite vacuole (pH 5.1) the metallic hybrid accumulates in aqueous phase so it can act as a good antimalarial agent.

Biological studies of CQPQ-gold(I) hybrid molecule

The growth inhibitory IC_{50} values on the asexual blood stage of *P. falciparum* were determined against CQ-susceptible 3D7 and CQ-resistant W2 strains (Table 4). CQPQ-gold(I) hybrid presented activity in low nanomolar range against the susceptible *P. falciparum* strain 3D7, being almost as potent as CQ, and 1000-folds more potent than PQ. Against the resistant *P. falciparum* strain W2, CQPQ-gold(I) hybrid was at very least twice as potent

Table 4. Cytostatic activity against the intraerythrocytic *P. falciparum* stage, mammalian cell cytotoxicity and selectivity indexes of compounds.

Compounds	*P. falciparum*, IC_{50} ± S.D. [μM][a]		Cells, CC_{50} ± S.E.M. [μM][b]		Selectivity index[c]	
	CQ-sensitive 3D7	CQ-resistant W2	J774	HepG2	3D7	W2
PQ	1.1173 ± 0.05	0.1823 ± 0.0189	24.6 ± 1.05	25.4 ± 2.65	22	135
CQ	0.018 ± 0.00167	0.460 ± 0.0174	51.5 ± 1.86	~80	2861	112
CQPQ-gold(I) hybrid	0.0277 ± 0.0039	0.166 ± 0.0257	20.9 ± 1.05	21.4 ± 7.5	753	126
$AuCl(PPh_3)$	> 2.0	–	19.74	4.53	–	–

[a] Determined 72 h after incubation with compounds. Values were calculated as mean of five independent experiments. [b] Determined 72 h after incubation with compounds. Values were calculated as mean of at least two independent experiments. IC_{50} = inhibitory concentration at 50%. CC_{50} = cytotoxic concentration at 50%. S.D. = standard deviation. S.E.M. = standard error of the mean. [c] Determined as CC_{50} (J774 cells) /IC_{50}.

as CQ and as potent as PQ. Regarding cell toxicity, CQPQ-gold(I) hybrid presented a profile similar to PQ, being toxic in concentration equal or above 20 μM. As a result, the selectivity index of the metallic hybrid was similar to that of PQ and twice lower than CQ. Based on this, it can be stated that CQPQ-gold(I) hybrid has conserved the potency of CQ against the susceptible strain, and equally important, also retained the beneficial profile of PQ against the resistant strain of *P. falciparum*. Moreover, the evaluation of the interaction between these compounds and the red blood cells at 20 μM concentration, equivalent to 1000-fold of the IC_{50} of CQPQ-gold(I) hybrid, the hemolysis was at 10% indicating no interaction with red blood cells at the proposed treatment concentration and presenting an acceptable safety profile (Figure S22).

After having ascertained the activity of the metallic hybrid at the blood stage, the growth inhibitory IC_{50} values on the liver stage using *P. berghei* sporozoites-infected Huh-7 cells were determined (Table 5; Figure 7). In this parasite stage CQ has a very weak potency, while PQ has moderate. In contrast, CQPQ-gold(I) hybrid has been shown to be very potent, approximately 10-fold more than PQ. The enhanced potency of the CQPQ-gold hybrid at the liver stage in comparison to PQ led us to analyze the course of infection and the profile of parasite morphology following treatment (Figure 8). To this end, Huh-7 cells were infected with *P. berghei* sporozoites and treated with PQ or with CQPQ-gold(I) hybrid. After 24 h of treatment, parasites were imaged by transmission electron microscopy (TEM) and parasite burden as well as morphology were analyzed. In comparison to the untreated parasite control, the treatment with PQ and with the CQPQ-gold(I) hybrid at the same concentration reduced the parasite burden. This reduction induced by our metallic hybrid was approximately twice greater than by PQ. The course of infection imaged by TEM revealed that in comparison to uninfected Huh-7 cells, which typically exhibited large and intact nuclei, untreated infected cells presented fragmented nuclei and a number of schizonts surrounding cell membrane as well as being released. A close inspection of the morphology revealed that PQ treatment was able to delay the course of infection, where most the Huh-7 cells presented parasites arrested in the transition from sporozoites into schizonts. The treatment with the metallic hybrid resulted in the most efficient delay in the course of infection, where most of the Huh-7 cells presented parasites arrested in the sporozoite stage. It can be concluded that the hybrid acts on liver stage in a manner

Table 5. Antiparasitic activity of compounds in inhibiting of *P. berghei*-sporozoite development in Huh-7 cells.

Compounds	Sporozoites-infected cells, IC_{50} ± S.D. [μM][a]	Cells, CC_{50} ± S.E.M. [μM][b]	
		J774	HepG2
PQ	~10	24.6 ± 1.05	25.4 ± 2.65
CQ	~15	51.5 ± 1.86	~80
CQPQ-gold(I) hybrid	0.63 ± 0.07	20.9 ± 1.05	21.4 ± 7.5

[a], [b] See footnotes in Table 4.

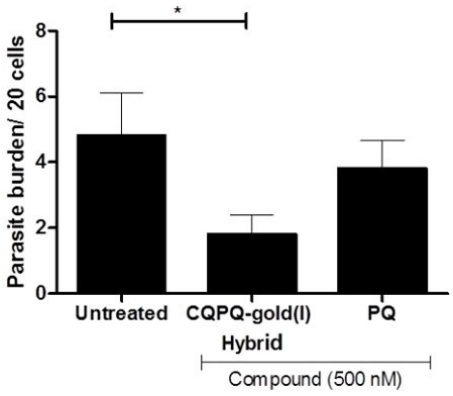

Figure 7. Quantification of parasite burden in the *P. berghei* sporozoite-infected Huh-7 cells. * $p < 0.01$ (one-way ANOVA).

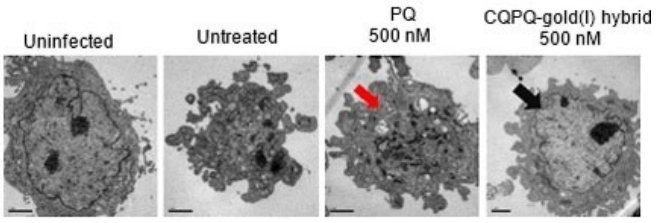

Figure 8. Transmission electron microscopy micrographs of Huh-7 cells, uninfected or infected with *P. berghei* sporozoites with no treatment or treated with primaquine or the CQPQ-gold(I) hybrid. Uninfected Huh-7 cells typically exhibited large and intact nuclei. Untreated infected cells presented fragmented nuclei and a number of schizonts surrounding the cell membrane, as well as being released. Huh-7 cells after treatment with CQPQ-gold(I) hybrid at 500 nM concentration 24 h post-infection have intact nuclei and healthy morphology (black arrow). Cells treated with primaquine under the same conditions presented diffuse parasites without a delimited membrane (red arrow). Scale bars: 2 μm.

similar to PQ, and it blocks the transition of sporozoites into schizonts, but with a superior potency. Considering that PQ is extensively metabolized that explains its modest activity on liver stage,[13,56] the enhanced potency of the CQPQ-gold(I) hybrid is likely due to the presence of the gold atom attached to PQ, which either affects the undesirable metabolism or enhance the PQ uptake.

After demonstrating the potency of the CQPQ-gold(I) hybrid against the parasite on both the blood and liver stages, we tested its efficacy against malaria in mice experiments. In the Peters suppressive test of parasitemia the metallic hybrid presented strong efficacy in reducing parasitemia and increasing mice survival when applied at the highest dose (33 μmol/kg). The same dose of CQ cured only 20% of the mice, while the metallic hybrid cured 100%. The efficacy of the CQPQ-gold(I) hybrid in curing mice was greater than PQ at a twofold dose, meaning that it is higher than CQ or PQ alone to confirm this finding, an experimental group also received an equimolar mixture of PQ and CQ (denoted here as CQPQ). The results show that our metallic hybrid at 33 μmol/kg dose was even more effective in curing mice than CQPQ at dose of 66 μmol/kg confirming that CQPQ-gold(I) hybrid has superior efficacy in suppressing the onset of infection (Table 6).

Next, we assessed if CQPQ-gold(I) hybrid can demonstrate efficacy in an established experimental infection setting (Thompson test), where treatment is given for mice displaying a patent parasitemia of 3–5% (Figure 9 A). In this experiment, the treatment with hybrid at 49 μmol/kg dose significantly reduced parasitemia and increased mice survival in comparison to untreated infected group (vehicle). In contrast, a similar efficacy was only observed with CQPQ at 66 μmol/kg dose, again denoting the higher efficacy of the metallic hybrid than CQPQ (Figure 9B and C; Table 7). The treatment with CQPQ-gold(I) hybrid ($[AuCQPQ]PF_6$) proved to be efficacious in reducing parasitemia and increasing survival of mice. However, it did not cure mice for good, suggesting that a successful therapy of an already established infection should also contain a fast-killing antimalarial component.[57] It is well-known that neither CQ nor PQ is a fast-killing antimalarial agent.[58] The observation from the Thompson test results indicates that the enhanced potency and efficacy of the CQPQ-gold(I) hybrid are not due to a rapid rate-of-kill property enhancement.

Table 6. Efficacy evaluation of CQPQ-gold(I) hybrid in suppressing parasitemia in *P. berghei*-infected mice.

Compound	Dose μmol/kg [mg/kg]	Inhibition parasitemia [%][a]	Median survival [days]	Number of mice alive after 40 dpi [%][b]
saline (vehicle)	–	–	20.3	0/15 (0)
CQ	33 (11)	>99	27	1/5 (20)
PQ	77 (20)	>99	>41	3/5 (60)
CQPQ	66[c]	>99	>41	4/5 (80)
$[AuCQPQ]PF_6$	33 (30)	>99	>41	5/5 (100)
	11 (10)	71.8±4.9	40	5/10 (50)
	3.6 (3.3)	5±3.9	n.d.	0/5 (0)

[a] Values compared to vehicle group, errors are standard deviation. [b] DPI = days post-infection. [c] Ratio of 1:1 of CQ and PQ, using 33 μmol/kg each.

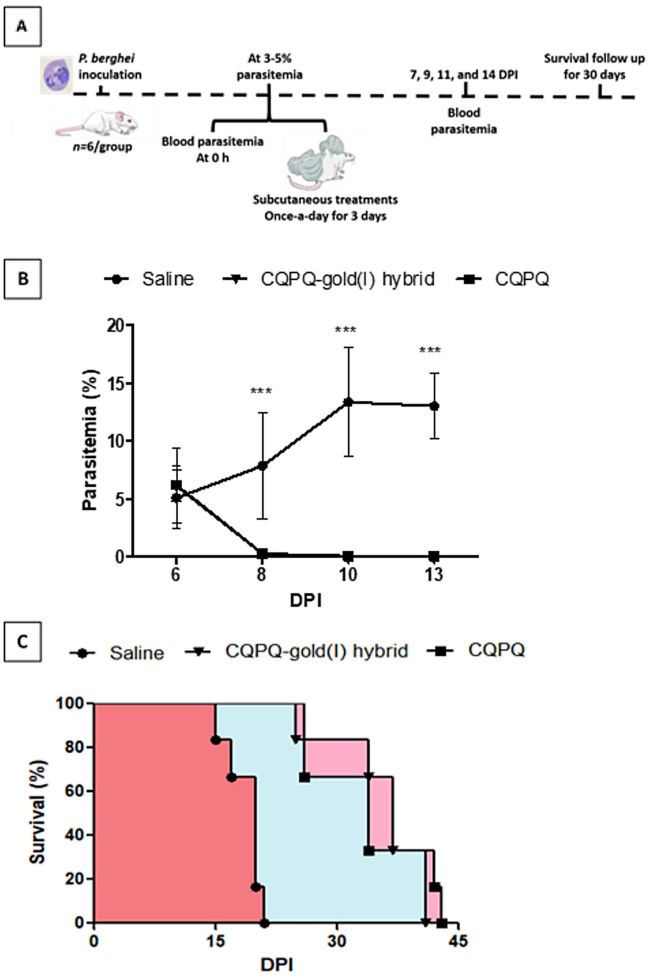

Figure 9. Evaluation of the efficacy of different compounds on *P. berghei*-infected mice in an established infection experimental setting (Thompson test). A) Experimental design of curative Thompson test, B) curve of parasitemia, and C) animal survival of *P. berghei*-infected mice. Parasitemia and animal survival were measured by using an $n=6$/group. Error bars indicate S.D. *** $p<0.01$ (two-way ANOVA) versus vehicle group. DPI = days post-infection.

Table 7. Survival evaluation of mice treated with compounds in an stablished infection experimental (Thompson test).

Compound	Dose [μmol/kg]	Median survival [days]	Number of mice alive after 40 dpi [%][a]
saline (vehicle)	–	20	0/6 (0)
CQPQ[b]	66	34	0/6 (0)
CQPQ-gold(I) hybrid	49	37	0/6 (0)

[a] DPI = days post-infection. [b] Ratio of 1:1 of CQ and PQ, using 33 μmol/kg each.

Earlier the CQPQ-gold(I) hybrid demonstrated potent inhibition of the β-hematin formation in aqueous phase, similar to CQ, meanwhile, it was substantially more potent than CQ at the aqueous/*n*-octanol interface. This pointed out that the hybrid conserved the inhibition potency of CQ and that it displayed a fine-tuned distribution along digestive vacuole. Because of its

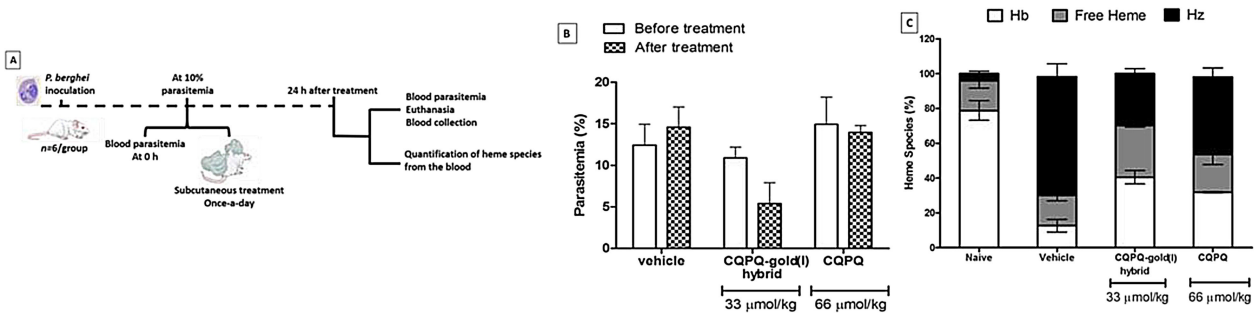

Figure 10. A) Experimental design, B) parasitemia, C) heme species, and summary of results (Table 8) from *P. berghei*-infected mice within 24 h of oral treatment. In (B), parasitemia was determined by GFP signal using flow cytometry. In (C), heme species were quantified from the peripheral blood after mouse euthanasia. Results show the pool of two independent experiments for $n = 3$/group for each experiment. Error bars are mean and 95% CI. $^{*}p < 0.05$ (one-way ANOVA and Newman-Keuls Multiple comparison test) between before versus after drug treatment. Hb, Hemoglobin; Hz, Hemozoin. CI = confidence interval.

inhibitory effect on hemozoin biosynthesis, the CQPQ-gold(I) hybrid demonstrated superior antimalarial potency and efficacy on the blood stage, which is a hallmark of the CQ treatment. This was investigated in *P. berghei*-infected mice by simultaneous monitoring of parasitemia and three heme species: hemoglobin, free heme and hemozoin (Figure 10 A). These experiments revealed that 24 h after administration of a single subcutaneous dose of 33 μmol/kg, CQPQ-gold(I) hybrid reduced parasitemia by 55.0 ± 8.7% and it was effective in impairing hemozoin formation by 44.2 ± 4.8% compared to untreated mice (Table 8). The treatment with 66 μmol/kg, 2-fold the dose of hybrid, showed that CQPQ did not reduce parasitemia, but it did significantly reduce hemozoin by 50.2 ± 10.0% (Table 8; Figure 10B and C). Concomitant to the decrease in the hemozoin levels, both CQPQ and CQPQ-gold(I) hybrid increased the levels of free heme, clearly showing that the treatment is efficient in interrupting the biosynthesis of hemozoin.

Table 8. Summary of results from *P. berghei*-infected mice after 24 h of subcutaneous treatment.

Treatment [dose, μmol/kg]	Inhibition [%][a] Parasitemia	Hemozoin	Free heme increase [%][a]
CQPQ-gold(I) hybrid (33)	55.0 ± 8.7	44.2 ± 4.8	38.4 ± 4.3
CQPQ (66)	0	50.2 ± 10.0	44.4 ± 7.9

[a] Compared to vehicle.

Once we ascertained that the superior potency and efficacy of CQPQ-gold(I) hybrid is in part due to its remarkable ability in simultaneously reducing parasitemia and modulating hemozoin formation, we investigated the effect of the primaquine component of CQPQ-gold(I) hybrid on the antiparasitic activity at the blood-stage. To this end, we determined the antiparasitic activity *in vitro* in cultured *P. berghei* and estimated the binding of compounds to reduced glutathione (GSH). We also investigated the ability of CQPQ-gold(I) hybrid and CQPQ combination to block or delay the maturation of *P. berghei* from rings to schizonts with *in vivo* Peters and Thompson tests. The CQPQ-gold(I) hybrid has reduced parasitemia by 50% at high and moderate concentrations in comparison to the untreated, unlike CQPQ which show potential on the rings only at fourfold concentration (1000 nM) (Figure 11 A and B). Moreover, in *in vitro* tests with *P. berghei* only CQPQ-gold(I) hybrid demonstrated activity at the common concentrations among the compounds (Figure 11 C). These findings suggest that the coordination of CQ and PQ to a gold ion and the creation of one single molecule is key to the enhanced antiparasitic activity that has been consistently demonstrated in both *in vitro* and *in vivo* models. It is likely due to the optimized pharmacodynamics rather than optimized pharmacokinetics. Furthermore,

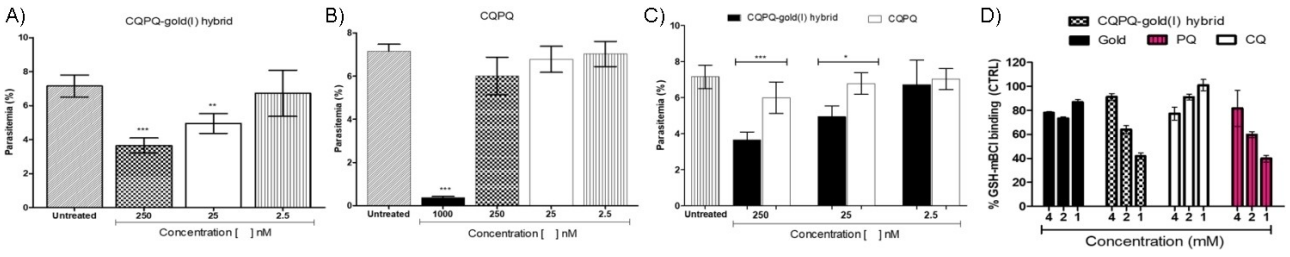

Figure 11. *In vitro* evaluation of the ability of CQPQ-gold(I) hybrid and CQPQ combination to block or delay of the maturation of *P. berghei* from rings to schizonts and the binding of compounds to reduced glutathione. A) The hybrid and B) CQPQ were tested at different concentrations on rings of *P. berghei*. C) The hybrid and CQPQ were tested at different concentrations, and the parasitemia was quantified; error bars indicate S.D. $^{***}p < 0.0002$ and $^{**}p < 0.001$ (one-way ANOVA) for hybrid or CQPQ versus untreated group and hybrid versus CQPQ. D) CQ, PQ or hybrid binding was measured by interaction with GSH in a cell-free assay.

we also observed that, unlike CQ, the CQPQ-gold(I) hybrid and PQ are able to interact with GSH in a cell-free assay (Figure 11 D), suggesting that the primaquine component of the metallic hybrid plays an important role in the blood-stage antiparasitic activity mediated by GSH depletion.

Conclusion

The novel CQPQ-gold(I) hybrid molecule synthesized in this work is a multitarget drug that interacts with DNA, inhibits the β-hematin formation, and also displays potent antiparasitic activity and selectivity against two different stages of malaria, the liver and the blood (asexual) stages. Regarding the liver stage of *P. berghei* infection, the CQPQ-gold(I) hybrid presented significantly better potency compared to PQ, while CQ was not active at all. In the blood stage of infection, the CQPQ-gold(I) hybrid was as potent against a sensitive *P. falciparum* strain as CQ, and against a CQ-resistant strain it was as potent as PQ. In the experimental malaria infection model, this metallic hybrid exhibited superior efficacy to CQ and PQ and even to a combination of both. This synergistic effect is in part explained by the fact that the [AuCQPQ]PF_6 hybrid successfully combines the CQ ability to impair the hemozoin formation with the ability to reduce parasitemia in a dose range where both quinolines drugs are ineffective. In-silico assays suggested that $[AuCQPQ]^+$ interacts moderately with the DNA minor groove. In addition, the binding mode of $[AuCQPQ]^+$ with PfTrxR was also predicted and showed the CQ portion within the interface cavity towards the N-terminal region of the enzyme. Overall, the binding to the enzyme was 1.2 times stronger than DNA binding, suggesting the PfTrxR enzyme is a potential target for our CQPQ-gold(I) hybrid, and that the CQ ligand essential for binding both targets. Collectively, our data suggest that gold(I) linked to two quinoline drugs (CQ and PQ) explains the observed improved potency and efficacy, a feature which cannot be observed when only CQ and PQ are given together. The findings are in support of the idea that CQPQ-gold(I) hybrid presents more potential in the antimalarial intervention than in a combined therapy.

Experimental Section

Materials and methods

All reactions were made using Schlenk techniques[59] and the solvents were distilled using the appropriate distilling agents.[60] All reagents were used as received with no further purification. The extraction of chloroquine base and PQ base from their diphosphate salts were performed according to the literature.[61] The THT–Au–Cl was synthetized as described in the literature.[62] The NMR spectra were obtained at 298 K in [D_6]DMSO solution employing a Bruker Avance III HD 500 spectrometer, 9.4 T and the spectra were calibrated using deuterated solvent. The IR spectra were obtained in a Bruker Alpha FT-IR Spectrometer in the region of 4000–400 cm^{-1} with a spectral resolution of 4 cm^{-1}. All UV/Vis experiments were performed on UV-1800 Spectrophotometer Shimadzu using quartz cuvettes. The mass spectroscopy experiments were performed on an AXIMA Performance matrix assisted laser desorption/ionization time of flight (MALDI-TOF) from Shimadzu Biotech, employing a nitrogen laser (λ_{max} = 337 nm) for excitation in an α cyano matrix. Elemental analyses were obtained in a Perkin Elmer 2400 CHNS/O Series II microanalyzer. The conductivity data were obtained in a Meter Lab CDM2300 instrument and fluorescence measurements were carried out using a Perkin Elmer LS45 spectrophotometer with a pulse xenon lamp.

Synthesis

AuPQCl: A solution of primaquine (535 mg, 1.99 mmol) in dichloromethane was added to a solution of Au(THT)Cl (400 mg, 1.25 mmol) previously synthesized in dichloromethane, and the solution remained in stirring for 2 h at 0 °C. The solvent was evaporated under vacuum and after diethyl ether addition, the solvent was evaporated again and the complex was obtained as a solid. The complex was washed with diethyl ether and dried under vacuum.

[AuCQPQ]PF_6: (CQPQ-gold(I) hybrid): A solution of AuPQCl (153 mg, 0.31 mmol) in acetonitrile (10 mL) was added to NH_4PF_6 (90 mg, 0.56 mmol) the mixture was stirred for 2 h. The solution was then filtered through celite and added drop by drop in a solution of chloroquine (127 mg, 0.40 mmol) in acetonitrile (10 mL). After 4 h of agitation at 0 °C, the solvent was evaporated and brown oil was obtained. After washing by diethyl ether and evaporation, the brown precipitated product was washed with three portions of diethyl ether and dried under vacuum. Yield: 73%; Molar conductivity in DMSO, $\Lambda_M = 39.18 \pm 0.06$ $ohm^{-1}cm^2mol^{-1}$. ^{1}H NMR ($(CD_3)_2SO$) ppm 8.54 (dd, J = 1.5 Hz, 4 Hz, Hb); 8.35 (m, H2, H5); 8.07 (dd, J = 8 Hz, J = 1.5 Hz, Hd); 7.77 (d, J = 2, H8); 7.42 (m, Hc,H6); 6.94 (d, J = 7.5 Hz, N**2**H); 6.52 (d, J = 5 Hz, H3); 6.49 (d, J = 2 Hz, Hg); 6.29 (d, J = 2 Hz, He); 6.15 (N**b**H); 3.82 (s, Hl); 3.76 (m, H1′); 3.67 (m, Ha′); 2.76 (m, Hd′, H4′, H5′); 1.57 (m, Hb′, Hc′, H2′, H3′); 1.22 (m, Ha″, H1″); 1.05 (t, J = 7 Hz, H6′); ^{13}C{^{1}H} NMR ($(CD_3)_2SO$) ppm 158.99 (Cf);151.75 (C2); 149.60 (C4); 149.07 (C9); 144.61 (Ci); 144.27 (Cb); 134.85 (Cd); 134.55 (Ch); 133.47 (C7); 129.61 (Cj); 127.30 (C8); 124.35 (C5);123.90 (C6); 122.15 (Cc); 117.47 (C10); 98.88 (C3); 96.29 (Ce); 91.73 (Cg); 55.01 (Cl); 51.31 (C4′); 47.41 (C1′); 46.81 (Ca′); 46.25 (C5′); 39.51 (Cd′); 32.75 (C2′, Cb′); 24.01 (Cc′); 21.61 (C3′); 20.27 (Ca″); 19.83 (C1″); 9.80 (C6′). ^{31}P{^{1}H} NMR PF_6^- ppm −144.2 (hep). IR ν (N–H) 3634, 3211; ν (NH_2) 3422, 3305; ν (C=C) 1615; ν(C=N) 1580; ν (PF_6) 844; ν(Au–N) 557. λ_{max} nm in DMSO (ε, $M^{-1}cm^{-1}$): 340 (11767). MS (MALDI) (m/z) calcd for $[Au\text{-}PQ]^+ = 456.14$ $[CQ+H]^+ = 320.19$; found 456.14; 320.15; elemental analysis calcd. (%) for $C_{33}H_{47}AuClF_6N_6OP$.*3/2* $C_4H_{10}O$.*3/2*CH_3CN: C 46.11, H 6.13, N 9.60; found: C 46.41, H 5.71, N 9.56.

Biotargets – metallic hybrid interaction studies

DNA as a target

Spectrophotometric titrations: Absorption titration experiments were carried out by stepwise additions of the calf thymus DNA (CT-DNA) solution (1.38 mM, in 5 mM Tris·HCl, pH 7.54 and 50 mM NaCl buffer) to the solution of each compound (0.4 μM) in DMSO, recording the UV/Vis spectra after each addition. Native DNA absorption was subtracted by adding the same amounts of CT-DNA to the blank cell. The binding affinity (K_b) was calculated from the spectrophotometric data according to the equation.[63]

$$\frac{[DNA]}{(\varepsilon_a - \varepsilon_f)} = \frac{[DNA]}{(\varepsilon_0 - \varepsilon_f)} + \frac{1}{Kb(\varepsilon_0 - \varepsilon_f)}$$

Where [DNA] is the concentration of DNA in base pairs, ε_a is the extinction coefficient of the observed absorption band at the given DNA concentration (corresponding to A_{obs}/[compound]), ε_f is the extinction coefficient of the free compound in solution, and ε_b is the extinction coefficient of the compound when fully bound to DNA. A plot of [DNA]/[$\varepsilon_a-\varepsilon_f$] versus [DNA] gave a slope 1/[$\varepsilon_a-\varepsilon_f$] and a *y* intercept of 1/K_b[$\varepsilon_b-\varepsilon_f$]. K_b is the ratio of the slope to the intercept.

Viscosity study: Viscosity measurements were carried out using an Ostwald viscometer immersed in a water bath maintained at 25 °C. The DNA concentration in buffer Tris·HCl was kept constant in all samples, however the [AuCQPQ]PF_6 hybrid concentration was increased from 0 to 147 μM. The flow time was measured at 3 times with a digital chronometer and the value was expressed as the mean. Data are presented as $(\eta/\eta_0)^{1/3}$ versus the ratio [complex]/[DNA], where η and η_0 are the specific viscosity of DNA with the metallic hybrid and alone, respectively. The specific viscosity values were calculated using $(t-t_b)/t_b$, where *t* is the observed flow time and t_b is the flow time of buffer.

Competitive DNA-binding studies: Ethidium bromide displacement assay was carried out essentially as per literature.[64] The maximum quantum yield for ethidium bromide was achieved at 471 nm; so this wavelength was selected as the excitation radiation for all samples at room temperature and in the emission range of 500–750 nm. The CT DNA-EB complex was prepared by adding 50 μL EB (1 mM) and 100 μL CT DNA (2 mM) in 5 mL of buffer (50 mM NaCl and 50 mM trizma at pH 7.3). The influence of the addition of each compound to the DNA–EB system solution was obtained by recording the variation of fluorescence emission spectra. [AuCQPQ]PF_6 hybrid did not exhibit emission in the presence of DNA and it did not influence the emission intensity of the free EB in the absence of DNA. Thus, the competitive DNA binding of the complex with EB could provide an evidence for interaction of the metallic hybrid with DNA base pairs. To quantify the affinity of the binding of the studied compound to DNA, the intrinsic binding constant (K_b) of the compound to DNA were obtained using the equation.

$$\frac{r}{Cf} = K_b x(n-r)$$

$C_b = C_t[(F-F_0)/(F_{max}-F_0)]$; where C_t is the total compound concentration, *F* is the observed fluorescence emission intensity at a given DNA concentration, F_0 is the intensity in the absence of DNA, and F_{max} is the fluorescence of the totally bound [AuCQPQ]PF_6 hybrid. Binding data were graphed as a Scatchard plot of r/C_f versus *r*, where r is the binding ratio C_b/[DNA]*t*, C_f is the free [AuCQPQ]PF_6 hybrid concentration and *n* is the number of binding sites.

Electrophoresis: For the DNA electrophoresis assays, 10 μL samples of the pBR322 plasmid (20 μg/mL) were combined with the [AuCQPQ]PF_6 hybrid at different ratios (molar ratios of [AuCQPQ]PF_6 hybrid / DNA (Ri) 1–4) and then incubated for 18 h at 37 °C. The reaction was then quenched by the addition of NaCl (1 M) to give a final chloride concentration of 0.2 M. Each sample (5 mL) was run (100 V for 40 min.) on a 0.7% agarose gel with TBE 1X (0.45 M Tris·HCl, 0.45 M boric acid, 10 mM EDTA) and stained with ethidium bromide. The bands were then viewed with a transilluminator and the image captured using a camera CoolSnapHQ2 (BIO-RAD), Universal HOOD III model 30.

Heme as a target

Interaction with ferriprotoporphyrin (Fe^{III}PPIX): The association constant of [AuCQPQ]PF_6 hybrid with ferriprotoporphyrin IX (hemin) was determined in 40% aqueous-DMSO as described previously.[65] The hemin stock solution (pH 7.5) were prepared with 3.5 mg of hemin in 10 mL of DMSO and the solution of Fe^{III}PPIX in 40% DMSO, were prepared with 140 μL of this hemin stock solution, 5 mL of distilled water, 3.86 mL of DMSO and 1 mL of 0.2 M Tris buffer (Tris; Tris(hydroxymethyl)aminomethane). CQPQ-gold(I) hybrid solution was prepared in 40% DMSO and aliquots of this solution was added to Fe^{III}PPIX and blank solutions in order to subtract the absorbance of the drug. The absorbance in Soret band (402 nm) was measured in presence and in absence of complex solution and the binding affinity was determined using the data and the equation $A = (A_0 + A_\infty K[C])/(1 + K[C])$ for a 1:1 complexation model using nonlinear least squares fitting, A_0 is absorbance of Fe^{III}PPIX, A_∞ is the absorbance of the gold drug-hemin adduct at saturation and K is the association constant. The experiment measurements were made in triplicate.[66]

Determination of inhibition of β-hematin formation by infrared spectroscopy: The evaluation of the conversion of hemin to β-hematin was made as described by Egan et al.,[50] where 20 mg of hemin and two equivalents of the compound of interest were dissolved in 3 mL of 0.1 M NaOH solution and stirred for 30 minutes at 60 °C, then 0.3 mL of HCl 0.1 M solution and 1.7 mL of acetate buffer (10 M, pH 5) were added at the same temperature. After 120 min the mixture was cooled on ice for 10 min, centrifuged and washed with water to remove acetate salts. The solid was dried and infrared spectra were obtained with KBr pallets. Primaquine and chloroquine were used as negative and positive controls, respectively.[67]

Inhibition of β-hematin formation in buffer and interface: The assay of IC_{50} of the β-hematin formation in buffer was performed as per Dominguez.[68] Briefly, a solution of hemin (50 μL, 4 mM), dissolved in DMSO, was distributed in 96-well microplates. The CQPQ-gold(I) hybrid was dissolved in DMSO and added in triplicate in test wells (50 μL) to final concentrations of 0–20 mM/well. Controls contained water and DMSO. Hemozoin formation was initiated by the addition of acetate buffer (100 μL of 0.2 M, pH 4.4). Plates were incubated at 37 °C for 48 h to allow completion of the reaction and centrifuged at 4000 RPM × 15 min. After discarding the supernatant, the pellet was washed twice with DMSO (200 μL) and finally dissolved in NaOH (200 μL, 0.2 N). The solutions were further diluted to 1:2 with NaOH (0.1 N) and absorbance recorded at 405 nm. The results were expressed as a percentage of inhibition of hemozoin formation.

β-Hematin formation at a water/octanol interface was followed with a method modified by Martínez et al..[53] Hemin was dissolved in 0.1 M NaOH solution to generate hematin. Acetone was added until the acetone to water ratio reached 4:6; the final solution contained 15 mg hematin/mL. A sample of this solution (200 μL) was carefully introduced close to the interface between *n*-octanol (2 mL) and aqueous acetate buffer (5 mL, 8 M; pH 4.9) in a cylindrical vial with an internal diameter of 2.5 cm. The mixture was incubated at 37 °C for 2 h, and at the end of the incubation the product (β-hematin) was isolated by centrifugation. The pellet was collected and washed twice with DMSO (2 mL), centrifuged again for 20 min, washed with 2 mL of ethanol and then dissolved in 25 mL of 0.1 M NaOH for spectrophotometric quantification. For the measurements of heme aggregation inhibition activity the appropriate amount of the CQPQ-gold(I) hybrid (23 mM in DMSO) was dissolved; after stirring for 30 min to equilibrate the drug between the two phases, the hematin solution was added close to the interface and the procedure was followed as described above. All experiments were performed in triplicate.

Molecular modeling studies of the interaction of metallic hybrid with *P. falciparum* thioredoxin reductase enzyme and DNA

Quantum mechanical calculations: The 3D structure of [AuCQPQ]PF_6 was estimated by density functional theory calculation. The geometry was optimized in solution (using PCM approach) at B3LYP/SDD(f)/6-31 + G(2df) level. The same computational protocol was successfully applied for Au^{I} and Au^{III} complexes in our previous studies.[69–75] The vibrational frequencies were also calculated at the very same level of theory and the force constants estimated from the Hessian matrix using the Seminario method,[76] as implemented in the Visual Force Field Derivation Toolkit (VFFDT) program.[77] The final calculated geometry was also used to predict atomic charges (at HF/ SDD (f)/6-31 + G(2df) level) and ^{1}H and ^{13}C NMR chemical shifts relative to TMS standard (at B3LYP/SDD(f)/6-31 + G(2df) level). All calculations were carried out in the Gaussian-09 Rev. D.01 program.[78]

Molecular docking studies: Firstly, the interaction of [AuCQPQ]PF_6 with the *P. falciparum* thioredoxin reductase was analyzed. The PDB code 4J56 crystal structure was reported[22] for the mutant $PfTrxR^{C535S}$, which was reconstructed for the native form with Cys535 at the C-terminal motif. The enzyme structure is a homodimer containing 1008 residues (monomer 1: 1–504 and monomer 2: 505–1008-numbering scheme used in our edited structure) and two $FADH_2$ molecules. The goal of the present molecular modeling study was to predict and quantify the binding mode between [AuCQPQ]PF_6 and the PfTrxR enzyme.

Molecular docking studies were conducted in order to obtain some ligand-enzyme structures. The protocol was applied as in our previous papers for docking Au complexes in TrxR enzyme,[20,79] but with an update in the parameters file of the GOLD program[80] to account for gold atom (Atom type = Au, van der Waals radius = 1.51 Å, K value = 0.1, Ionization potential = 20.521 eV, Polarizability = 0.0, Atomic weight = 196.97, Formal charge = 1.0, Geometry = CO (coordinated metal ion), Number of neighbors = 0. The Au was defined as donor (D) with coordination number 2 and 4 and coordination distance of 2.29 Å. The maximum hydrogen bond energy was set to −15 to −10 kcal mol^{-1} (same as Zn). The remaining parameters needed were set as for Zn (available in the original program).

The CHEMPLP function[81] was defined for scoring, and the docking searching used 100 GA runs setting to 200% of search efficiency. The C-terminal (Cys535 and Cys540; PDB numbering scheme) and N-terminal (Cys88 and Cys93; PDB numbering scheme) residues were used to define the centroid of the binding site (Figure S23A). The searching space covered a sphere of 15 Å around the centroid that included most of the interface cavity (Figure S23B).

Two different docking protocols were applied. The first one was carried out without any constraint and 100 ligand-enzyme poses were generated. In the second docking protocol, the same binding site definition was considered but the distance between S(Cys540; PDB numbering scheme) and Au was constrained within a 1.5–3.5 Å range. Technically, this means that if the S–Au distance is out of the boundaries the score is decreased by an amount proportional to the difference. This was done based on the most probable action mechanism of Au complexes as inhibitor of TrxR,[20,79] which passes through reaction of Au complex with Cys in the C-terminal motif.

Similar protocol was applied for the docking study of [AuCQPQ]PF_6 hybrid with the DNA. The structure of B-DNA dodecamer was taken from PDB ID: 1BNA.[82] The docking was performed over the entire DNA structure by defining the searching space as a 30 Å sphere centered at the geometric center of structure. In that way the minor and major grooves were mapped. The CHEMPLP scoring function was used to rank the 100 selected poses.

Molecular dynamics simulation: In order to improve the docking studies, the best selected poses were submitted to molecular dynamics (MD) simulations. The first step was to parametrize the classical potential GAFF2[83] for the gold coordination sphere. These parameters include atomic charges for all atoms, bond and angle force constants involving the first and second coordination spheres (Table S2) and van der Waals parameters for Au atom. Atomic charges were calculated at quantum mechanical level as described previously, but at Hartree-Fock (HF) level instead of B3LYP. The force constants were obtained at B3LYP level and for the van der Waals parameters the values adjusted for cisplatin (a Pt^{II} complex) were used as described in our previous publication.[84] The remaining parameters are available in the GAFF2 as implemented in the Amber package.[85] The force field ff14SB[86] was used for the enzyme and the TIP3P model for solvent. For DNA, the OL15 force field[87] was used. The system containing the [AuCQPQ]PF_6 and PfTrxR enzyme (or the DNA dodecamer structure) (in distinct docking modes) was neutralized and immersed in a solvent box containing ~36000 water molecules (~7000 for DNA). The MD protocol involved the following steps: i) optimization of the solute, keeping the solvent molecules fixed; ii) optimization of the entire system; iii) NVT heating up to 310.0 K for 500 ps long; iv) NPT density equilibration for 1 ns long and v) NVT production for 100 ns long. Only the production phase data (considering the system in thermodynamic equilibrium) were analyzed and used to calculate the interaction properties.

Distribution coefficient (D)

The water/*n*-octanol distribution coefficients were determined by the stir-flask method,[88,89] water-saturated *n*-octanol and *n*-octanol-saturated water were prepared by shaking equal volumes of *n*-octanol and water for one week and allowing the mixture to separate into the respective phases. A UV/Vis calibration curve for [AuCQPQ]PF_6 hybrid in *n*-octanol-saturated water in the 2–50 μM range was prepared. A mixture of 10 mL *n*-octanol and 10 mL water (each saturated in the other) was stirred for 1 h at 37 °C, after adding the sample to be analyzed. Once equilibrium was reached, the organic and aqueous phases were separated and centrifuged. Finally, the concentration of [AuCQPQ]PF_6 in each phase was measured spectrophotometrically to determine values for $\log D = \log$ [drug in *n*-octanol]/[drug in water]. Experiments were carried out three times.[90]

Biological studies of metallic hybrids

In vitro antimalarial activity: The two strains, one of which is 3D7, the CQ-susceptible strain (isolated in West Africa; obtained from MR4, VA, USA), and the other is W2, the CQ-resistant strain (isolated in Indochina; obtained from MR4, VA, USA), were maintained in culture in Roswell Park Memorial Institute medium (RPMI 1640, Invitrogen), supplemented with 10% human serum (Abcys S.A. Paris, France) and buffered with 25 mM 4-(2-hydroxyethyl)-1-piperazineethanesulfonic acid (HEPES) and 25 mM $NaHCO_3$. Parasites were grown in A-positive human blood (Etablissement Français du Sang, Marseille, France) under controlled atmospheric conditions that consisted of 10% O_2, 5% CO_2 and 85% N_2 at 37 °C with a humidity of 95%.

The two strains were synchronized twice with sorbitol before use,[51] and clonality was verified every 15 days through PCR genotyping of the polymorphic genetic markers **msp1** and **msp2** and microsatellite loci.[52,53]

Chloroquine and primaquine were re-suspended in water in concentrations ranging between 3.2 to 3231 nM and 3.9 to 20 μM, respectively. $[AuCQPQ]PF_6$ was resuspended in DMSO and then diluted in RPMI/DMSO (99:1, *v/v*) to obtain final concentrations ranging from 3.9 to 20.1 μM.

For *in vitro* isotopic microtests, 25 μL/well of anti-malarial drug and 200 μL/well of the parasitized red blood cell suspension (final parasitemia, 0.5%; final hematocrit, 1.5%) were distributed into 96 well plates. The plates were incubated for 72 h at 37 °C in controlled atmosphere at 85% N_2, 10% O_2, 5% CO_2. After thawing the plates, hemolyzed cultures were homogenized by vortexing the plates. The drug susceptibility assay was performed using the HRP2 ELISA-based assay Malaria Ag Celisa kit (ref KM2159, Cellabs PTY LDT, Brookvale, Australia) as previously described.[54] The concentration at which the drugs were able to inhibit 50% of parasite growth (IC_{50}) was calculated with the inhibitory sigmoid E_{max} model, with estimation of the IC_{50} through nonlinear regression using a standard function of the R software (ICEstimator version 1.2). IC_{50} values were validated only if the OD ratio (OD at concentration 0/OD at concentration max) was greater than 1.6 and the confidence interval ratio (upper 95% confidence interval of the IC_{50} estimation/lower 95% confidence interval of the IC_{50} estimation) was less than 2.0. IC_{50} are expressed as means of 5 experiments.

Cell toxicity: In 96-well plates, HepG2 or J774 cells were seeded ((4.0×104 in 100 μL per well) of RPMI and Dulbecco's modified Eagle's medium (DMEM), respectively. Drugs were added 24 h later in a volume of 100 μL of medium and the plates were incubated for 72 h at 37 °C and under 5% CO_2. Drugs were tested in seven concentrations (1.25–80 μM), each one in triplicate. Doxorubicin chloridrate (Eurofarma, São Paulo, Brazil) was used as positive control, while untreated cells were employed as negative controls. Bioluminescence readings were performed using Filtermax™ F3 & F5 Multi-Mode instrument (Molecular Devices) using the kit CellTiter-Glo® (Promega). Mean CC_{50} values were calculated using data from three independent experiments.

Hemolysis assay: Fresh uninfected human O^+ erythrocytes were washed three times with sterile phosphate-buffered saline (PBS), adjusted for 1% hematocrit and 100 μL dispensed in a 96-well round bottom plate. Then, 100 μL of drugs previously in DMSO and suspended in PBS were dispensed in the respective wells. Each drug was tested in seven concentrations (0.312–20 μM), assayed in triplicate. Untreated cells received 100 μL of PBS containing 1% (*v/v*) DMSO (negative control), while positive controls received saponin (Sigma-Aldrich) at 1% *v/v*. Plates were incubated for 1 h at 37 °C under 5% CO_2. Plates were centrifuged at 1500 rpm by 300 g for 10 min and 100 μL of supernatant were transferred to another plate, in which absorbance at 540 nm was measured using a SpectraMax 190 instrument. The % of hemolysis was calculated as follow: [(mean sample absorbance−mean negative control absorbance/mean positive control absorbance−mean negative control absorbance)]×100, and plotted against drug concentration generated using GraphPad Prism 5.01. Two independent experiments were performed.

Activity against P. berghei liver stage: The transgenic *P. berghei* parasites expressing green fluorescent protein (GFP) and firefly luciferase (Luc), (PbGFP-Luccon, parasite line 676 m1cl1) were freshly obtained through disruption of salivary glands of infected female *Anopheles stephensi* mosquitoes. Human hepatoma cell line Huh-7 was cultured in complete RPMI (RPMI-1640 medium supplemented with 10% (*v/v*) fetal bovine serum, 1% (*v/v*) nonessential amino acids, 1% (*v/v*) penicillin/streptomycin, 1% (*v/v*) glutamine, and 10 mM HEPES). Inhibition of hepatic infection was determined by measuring the luminescence intensity in Huh-7 cells infected with the firefly luciferase-expressing *P. berghei* parasites as previously described.[91] Briefly, for infection assays, Huh-7 cells (1.0×10^4 per well) were seeded in 96-well plates one day before drug treatment and infection. The medium was replaced by medium containing the appropriate concentration of each compound, approximately 1 h prior to infection with sporozoites. An amount of the DMSO solvent equivalent to that present in the highest compound concentration was used as control. Sporozoite addition was followed by centrifugation at 1800×*g* for 5 min. Parasite infection load was measured 48 h post infection by a bioluminescence assay (Biotium, Hayward, CA, USA). The effect of the compounds on the viability of Huh-7 cells was assessed by the AlamarBlue assay (Life), using the manufacturer's protocol.

Transmission electron microscopy of P. berghei liver stage: Huh-7 cells (1.0×10^5 per well) were seeded in 24-well plates. After drug treatment for 1 h, cells were infected with fresh sporozoites. After 24 h of incubation, cells were removed using trypsin, washed twice in PBS, then fixed with 2% formaldehyde and 2.5% glutaraldehyde (Electron Microscopy Sciences, Hatfield, PA, USA) in sodium cacodylate buffer (0.1 M, pH 7.2) for 40 min at room temperature. After fixation, cells were washed 3 times with cacodylate buffer and post-fixed with a 1.0% solution of osmium tetroxide containing 0.8% potassium ferrocyanide (Sigma-Aldrich) for 1 h. Cells were subsequently dehydrated in increasing concentrations of acetone (30, 50, 70, 90 and 100%) for 10 min in each step and embedded in Polybed resin (PolyScience family, Warrington, PA, USA). Ultrathin sections on copper grids were contrasted with uranyl acetate and lead citrate. Micrographs were taken using a JEM-1230 microscope (JEOL, Peabody, MA, USA).

Animals, parasites and reagents: Male Swiss Webster mice (18–22 g) were housed at Instituto Gonçalo Moniz (Fiocruz, Bahia, Brazil), maintained in sterilized cages under a controlled environment, receiving a rodent balanced diet and water ad libitum. All experiments were carried out in accordance with the recommendations of Ethical Issues Guidelines and were approved by the local Animal Ethics Committee (protocol number 02/2016). *P. berghei* expressing GFP was obtained as previously described[92] and kindly supplied by Prof. Antoniana Ursine Krettli (IRR/Fiocruz). Mitotracker™ deep red FM was purchased from Life Technology, ketamine and xylazine were purchased from Syntec (Sao Paulo, Brazil).

Suppressive activity (Peters test): Male Swiss Webster mice (18–22 g) were infected by intraperitoneal injection of 1×10^7 GFP-*P. berghei*-infected erythrocytes per mouse and randomly divided into groups of $n=5$. Each compound was solubilized in propylene glycol/saline (20:80, *v/v*) prior to administration and treatment was initiated 24 h post infection and given once a day for four consecutive days by subcutaneous injection of 100 μL into the skin over the neck. Untreated infected mice receiving propylene glycol/saline (20:80, *v/v*) were used as negative control (vehicle). Parasitemia was determined by flow cytometry using GFP signal and co-staining with Mitotracker™ deep red FM (33 ng/mL), animal survival was observed daily until 40 days post-infection. The % of parasitemia reduction was calculated as follow: [mean vehicle group−mean treated

group/mean vehicle group]×100. Experiments were independently repeated for drug doses which inhibited >80% the parasitemia.

Curative activity (Thompson test): Male Swiss Webster mice (18–22 g) were infected by intraperitoneal injection of 1×10^7 GFP–*P. berghei*-infected erythrocyte. Mice with parasitemia between 3–5% were randomly divided into groups of $n=6$ and treatment was performed daily for three consecutive days by subcutaneous route. Untreated infected mice receiving propylene glycol/saline (20:80, *v/v*) were used as a negative control (vehicle). The following parameters were evaluated: parasitemia counted at days 7, 9, 11 and 14 post-infection and 45 days post-infection animal survival. One experiment was performed.

Schizont maturation assessment: Male C57BL/6 mice (18–22 g) were infected by intraperitoneal injection of synchronized 1×10^7 GFP–*P. berghei*-infected erythrocytes per mouse and then the blood with 2–5% of parasitemia was collected. After successive washes with 0.9% sterile saline, 250 μL/well of GFP–*P. berghei*-infected blood was plated in 48-wells plate and the hematocrit adjusted to 2% when needed. Then, 250 μL/well of each compound solubilized in DMSO and diluted in RPMI medium in different concentrations (2.5, 25, 250 and 1000 nM) were dispensed in the respective wells in triplicate. The plate was maintained with a standard mixture of gases (3% O_2, 5% CO_2 and 91% N_2) and incubated at 37 °C for 24 h as described.[93] Untreated infected-blood was used as negative control. Parasitemia was determined by flow cytometry using GFP signal and co-staining with Mitotracker™ deep red FM (33 ng/mL). Three independent experiments were performed.

Inhibition of hemozoin biosynthesis: Male Swiss Webster mice (18–22 g) infected by *P. berghei* at parasitemia up to 10% were randomly divided into $n=3$/group. Treatment was performed by a single dose given by subcutaneous route. Untreated infected mice (vehicle) and uninfected mice (naïve) were included as control groups. Parasitemia was determined by flow cytometry before and after drug treatment. After 24 h treatment, mice were anesthetized using 70 mg/kg ketamine and 12.5 mg/kg xylazine (intraperitoneal), blood was gently aspirated in the brachial plexus using heparin coated tips and transferred into heparinized blood collection vials. Blood were centrifuged at 2500 rpm by 500 g at 4 °C for 5 min., plasma was discarded and cell pellet was washed with saline. Equal volumes of the remaining pellet were transferred to new tubes, suspended in 1.0 mL of 0.05% saponin and frozen overnight. Then, samples were centrifuged at 10000 rpmby 2500 g at 4 °C for 10 min., a volume of 0.5 mL of saline was added and centrifugation was repeated twice, the resulting cell pellets were processed to determining hemoglobin, free heme and hemozoin according to a previously described method.[94] At least two independent experiments were performed.

Binding to reduced glutathione: A solution of reduced glutathione (Sigma-Aldrich, 100 μL, 0.2 mM) dissolved in PBS pH 8.0 was distributed in a 96-well microplate. Testing compounds were dissolved in DMSO, diluted in PBS and then added in triplicate in the respective wells (50 μL) to final concentrations of 0.05 to 0.4 mM. Plate was incubated at 37 °C for 24 h to allow completion of the reaction, content was transferred into an opaque plate containing 20 μL of a solution of monochlorobimane at 1.0 mM. After 1 h of incubation at room temperature, fluorescence was recorded ($\lambda_{ex}=360$ nm, $\lambda_{em}=440$ nm). The results were expressed as a percentage of binding or inhibition in comparison to control without the testing compounds.

Acknowledgements

The authors are grateful to Dr. Roberto Rosas Pinho and Camila Condé for determining mass spectra, Mariana Borges for helping in the sporozoite assays and Dr. David Bátka for text editing. This work was supported by the Brazilian funding agencies: CAPES (grant no. 23038.006713/2013-88), CNPq (grant no. 305732/2019-6), FAPES grant number APP0088/2016) and Fiocruz/Inova (grant no.1642178247). MP was supported by grant PTDC-SAU-INF-29550-2017 (FCT, Portugal). HFDS and VS also thankful to FAPEMIG for the purchase of Nvidia graphics processing unit (GPU) used to speed up the MD simulations. CSP thanks CAPES for her Ph.D. scholarship.

Conflict of Interest

The authors declare no conflict of interest.

Keywords: chloroquine · DNA · gold · heme · malaria · primaquine

[1] World Health Organization (WHO), *Malaria.* March 2020. Accessed on 28.3.2020. https://www.who.int/malaria/en/.
[2] Y. Bansal, O. Silakari, *Eur. J. Med. Chem.* **2014**, *76*, 31–42.
[3] M. Ouji, J.-M. Augereau, L. Paloque, F. Benoit-Vical, *Parasite* **2018**, *25*, 24.
[4] A. Çapcı, M. M. Lorion, H. Wang, N. Simon, M. Leidenberger, M. C. B. Silva, D. R. M. Moreira, Y. Zhu, Y. Meng, J. Y. Chen, Y. M. Lee, F. Oliver, B. Kappes, J. Wang, L. Ackermann, S. B. Tsogoeva, *Angew. Chem. Int. Ed.* **2019**, *58*, 13066–13079.
[5] M. Lödige, L. Hiersch, *Int. J. Med. Chem.* **2015**, *2015*, 1–23.
[6] R. Oliveira, D. Miranda, J. Magalhães, R. Capela, M. J. Perry, P. M. O. Neill, R. Moreira, F. Lopes, *Bioorg. Med. Chem.* **2015**, *23*, 5120–5130.
[7] F. Bellot, F. Coslédan, L. Vendier, J. Brocard, B. Meunier, A. Robert, *J. Med. Chem.* **2010**, *53*, 4103–4109.
[8] K. N. Olafson, M. A. Ketchum, J. D. Rimer, P. G. Vekilov, *Proc. Natl. Acad. Sci. USA* **2015**, *112*, 4946–4951.
[9] J. G. Woodland, R. Hunter, P. J. Smith, T. J. Egan, *ACS Chem. Biol.* **2018**, *13*, 2939–2948.
[10] M. Navarro, W. Castro, C. Biot, *Organometallics* **2012**, *31*, 5715–5727.
[11] D. W. Wilson, C. Langer, C. D. Goodman, G. I. McFadden, J. G. Beeson, *Antimicrob. Agents Chemother.* **2013**, *57*, 1455–1467.
[12] I. Sutanto, S. Suprijanto, A. Kosasih, M. S. Dahlan, D. Syafruddin, R. Kusriastuti, W. A. Hawley, N. F. Lobo, F. O. Ter Kuile, *Clin. Infect. Dis.* **2013**, *56*, 685–693.
[13] G. Camarda, P. Jirawatcharadech, R. S. Priestley, A. Saif, S. March, M. H. L. Wong, S. Leung, A. B. Miller, D. A. Baker, P. Alano, M. J. I. Paine, S. N. Bhatia, P. M. O'Neil, S. A. Ward, G. A. Biagini, *Nat. Commun.* **2019**, *10*, 3226.
[14] A. R. Sannella, A. Casini, C. Gabbiani, L. Messori, A. R. Bilia, F. F. Vincieri, G. Majori, C. Severini, *FEBS Lett.* **2008**, *582*, 844–847.
[15] M. Navarro, F. Vásquez, R. A. Sánchez-Delgado, H. Pérez, V. Sinou, J. Schrével, *J. Med. Chem.* **2004**, *47*, 5204–5209.
[16] M. Navarro, W. Castro, M. Madamet, R. Amalvict, N. Benoit, B. Pradines, *Malar. J.* **2014**, *13*, 1–8.
[17] M. Navarro, H. Perez, R. A. Sanchez-Delgado *J. Med. Chem.* **1997**, *40*, 1937–1939.
[18] A. Ssemaganda, L. M. Low, K. R. Verhoeft, M. Wambuzi, B. Kawoozo, S. B. Nabasumba, J. Mpendo, B. S. Bagaya, N. Kiwanuka, D. I. Stanisic, S. J. Berners-Price, M. F. Good, *Metallomics* **2018**, *10*, 444–454.
[19] M. Navarro, W. Castro, S. González, M. J. Abad, P. Taylor, *J. Mex. Chem. Soc.* **2013**, *57*, 220–229.
[20] A. Garcia, R. C. Machado, R. M. Grazul, M. T. P. Lopes, C. C. Corrêa, H. F. Dos Santos, M. V. De Almeida, H. Silva, *J. Biol. Inorg. Chem.* **2016**, *21*, 275–292.

[21] A. Caroli, S. Simeoni, R. Lepore, *Biochem. Biophys. Res. Commun.* **2012**, *417*, 576–581.
[22] K. Fritz-Wolf, E. Jortzik, M. Stumpf, J. Preuss, R. Iozef, S. Rahlfs, K. Becker, *J. Mol. Biol.* **2013**, *425*, 3446–3460.
[23] J. L. Medina-Franco, M. A. Giulianotti, G. S. Welmaker, R. A. Houghten, *Drug Discovery Today* **2013**, *18*, 495–501.
[24] M. Navarro, W. Castro, A. Martínez, R. A. Martínez, *J. Inorg. Biochem.* **2011**, *105*, 276–282.
[25] M. Navarro, W. Castro, S. González, M. J. Abad, P. Taylor, *J. Mex. Chem. Soc.* **2013**, *57*, 220–229.
[26] J. D. S. Chaves, J. L. Damasceno, M. C. F. Paula, P. F. De Oliveira, G. C. Azevedo, R. C. Matos, M. C. S. Lourenço, D. C. Tavares, H. Silva, A. P. S. Fontes, M. V. De Almeida, *BioMetals* **2015**, *28*, 845–860.
[27] L. Glans, A. Ehnbom, C. De Kock, A. Martínez, J. Estrada, P. J. Smith, M. Haukka, R. A. Sánchez-Delgado, E. Nordlander, *Dalton Trans.* **2012**, *41*, 2764–2773.
[28] W. I. Sundquist, D. P. Bancroft, S. J. Lippard, *J. Am. Chem. Soc.* **1990**, *112*, 1590–1596.
[29] R. M. Silverstein, M. Webster, D. J. Kiemle, *Spectrometric Identification of Organic Compounds*, 7th ed., Wiley, **2005**, pp. 319.
[30] M. K. Nazeeruddin, S. M. Zakeeruddin, R. Humphry-Baker, R. Humphry-Baker, S. I. Gorelsky, A. B. P. Lever, M. Gratzel, *Coord. Chem. Rev.* **2000**, *208*, 213–225.
[31] V. A. Bloomfield, M. D. Crothers, I. Tinoco, *Physical Chemistry of Nucleic Acids*, 3rd ed., Harper & Row, **1974**, pp. 517.
[32] C. S. K. Rajapakse, A. Martínez, B. Naoulou, A. A. Jarzecki, L. Suárez, C. Deregnaucourt, V. Sinou, J. Schrével, E. Musi, G. Ambrosini, G. K. Schwartz, R. A. Sánchez-Delgado, *Inorg. Chem.* **2009**, *48*, 1122–1131.
[33] C. Biot, W. Castro, C. Y. Botté, M. Navarro, *Dalton Trans.* **2012**, *41*, 6335–6349.
[34] A. G. Quiroga, J. M. Pérez, E. I. Montero, J. R. Masaguer, C. Alonso, C. Navarro-Ranninger, *J. Inorg. Biochem.* **1998**, *70*, 117–123.
[35] G. Ibrahim, G. M. Bouet, I. H. Hall, M. A. Khan, *J. Inorg. Biochem.* **2000**, *81*, 29–34.
[36] R. W. Y. Sun, A. L. F. Chow, X. H. Li, J. J. Yan, S. S. Y. Chui, C. M. Che, *Cells. Chem. Sci.* **2011**, *2*, 728–736.
[37] A. Kellett, Z. Molphy, C. Slator, V. McKee, N. P. Farrell, *Chem. Soc. Rev.* **2019**, *48*, 971–988.
[38] L. Colina-Vegas, W. Villarreal, M. Navarro, C. R. De Oliveira, A. E. Graminha, P. I. D. S. Maia, V. M. Deflon, A. G. Ferreira, M. R. Cominetti, A. A. Batista, *J. Inorg. Biochem.* **2015**, *153*, 150–161.
[39] C. R. Brodie, J. G. Collins, J. R. Aldrich-Wright, *Dalton* **2004**, *21*, 1145–1152.
[40] J.-B. Lepecq, C. A. Paoletti, *J. Mol. Biol.* **1967**, *27*, 87–106.
[41] J. R. Lakowicz, *Principles of Fluorescence Spectroscopy*, 3rd., Springer, **2006**.
[42] D. Ajloo, M. E. Moghadam, K. Ghadimi, M. Ghadamgahi, A. A. Saboury, A. Divsalar, M. Sheikhmohammadi, K. Yousefi, *Inorg. Chim. Acta* **2015**, *430*, 144–160.
[43] M. Zampakou, M. Akrivou, E. G. Andreadou, C. P. Raptopoulou, V. Psycharis, A. A. Pantazaki, G. Psomas, *J. Inorg. Biochem.* **2013**, *121*, 88–99.
[44] A. Zianna, G. Psomas, A. Hatzidimitriou, E. Coutouli-Argyropoulou, M. Lalia-Kantouri, *J. Inorg. Biochem.* **2013**, *127*, 116–126.
[45] A. Banerjee, J. Singh, D. Dasgupta, *J. Fluoresc.* **2013**, *23*, 745–752.
[46] J. M. Fortune, N. Osheroff, *J. Biol. Chem.* **1998**, *273*, 17643–17650.
[47] I. Mitra, S. Mukherjee, V. P. Reddy, B. S. Dasgupta, J. C. Bose, K. S. Mukherjee, W. Linert, S. C. Moi, *RSC Adv.* **2016**, *6*, 76600–76613..
[48] A. Prisecaru, Z. Molphy, R. G. Kipping, E. J. Peterson, Y. Qu, *Nucleic Acids Res.* **2014**, *42*, 13474–13487.
[49] S. Pagola, P. W. Stephens, D. S. Bohle, A. D. Kosar, S. K. Madsen, *Nature* **2000**, *404*, 307–310.
[50] T. J. Egan, D. C. Ross, P. A. Adams, *FEBS Lett.* **1994**, *352*, 54–57.
[51] T. J. Egan, W. W. Mavuso, K. K. Ncokazi, *Biochemistry* **2001**, *40*, 204–213.
[52] T. J. Egan, *J. Inorg. Biochem.* **2006**, *100*, 916–926.
[53] A. Martínez, C. S. K. Rajapakse, D. Jalloh, C. Dautriche, R. A. Sánchez-Delgado, *J. Biol. Inorg. Chem.* **2009**, *14*, 863–871.
[54] M. N. Wenzel, A. F. Móska, V. Graziani, B. Aikman, S. R. Thomas, A. De Almeida, J. A. Platts, N. Re, C. Coletti, A. Marrone, G. Soveral, A. Cassini, *Inorg. Chem.* **2019**, *58*, 2140–2148.
[55] A. Martínez, C. S. K. Rajapakse, B. Naoulou, Y. Kopkalli, L. Davenport, R. A. Sánchez-Delgado, *J. Biol. Inorg. Chem.* **2008**, *13*, 703–712.
[56] L. Aguiar, M. Machado, M. Sanches-Vaz, M. Prudêncio, N. Vale, P. Gomes, *MedChemComm* **2019**, *10*, 221–226.
[57] G. W. Birrell, M. Chavchich, A. L. Ager, H. M. Shieh, G. D. Heffernan, W. Zhao, P. E. Krasucki, K. W. Saionz, J. Terpinski, G. A. Schiehser, L. R. Jacobus, G. D. Shanks, L. R. Jacobus, M. D. Edstein, *Antimicrob. Agents Chemother.* **2015**, 59, 170–177.
[58] L. M. Sanz, B. Crespo, C. De-Cózar, X. C. Ding, J. L. Llergo, J. N. Burrows, J. F. García-Bustos, F. J. Gamo, *PLoS One* **2012**, *7*, e30949.
[59] D. F. Shriver, M. A. Dredzon, *The Manipulation of Air-Sensitive Compounds*, 2nd ed., Wiley, **1986**.
[60] D. B. G. Williams, M. Lawton, *J. Org. Chem.* **2010**, *75*, 8351–8354.
[61] R. A. Sánchez-Delgado, M. Navarro, H. Pérez, J. A. Urbina, *J. Med. Chem.* **1996**, *39*, 1095–1099.
[62] R. Uson, A. Laguna, M. Laguna, D. A. Briggs, H. H. Murray, J. P. Fackler, *Inorg. Synth.* **1989**, *26*, 85–91.
[63] G. Scatchard, *Ann. N. Y. Acad. Sci.* **1949**, *51*, 660–672.
[64] A. J. Geall, I. S. Blagbrough, *J. Pharm. Biomed. Anal.* **2000**, *22*, 849–859.
[65] T. J. Egan, W. W. Mavuso, D. C. Ross, H. M. Marques, *J. Inorg. Biochem.* **1997**, *68*, 137–145.
[66] T. S. Macedo, W. Villarreal, C. C. Couto, D. R. M. Moreira, M. Navarro, M. Machado, M. Prudêncio, A. A. Batista, M. B. P. Soares, *Metallomics* **2017**, *9*, 1548–1561.
[67] T. S. Macedo, L. Colina-Vegas, M. Da Paixão, M. Navarro, B. C. Barreto, P. C. M. Oliveira, S. G. Macambira, M. Machado, M. Prudêncio, S. D'Alessandro, N. Basilico, D. R. M. Moreira, A. A. Batista, M. B. P. Soares, *Parasitology* **2016**, *143*, 1543–1556.
[68] J. N. Domínguez, C. León, J. Rodrigues, N. G. De Domínguez, J. Gut, P. J. Rosenthal, *Farmaco* **2005**, *60*, 307–311.
[69] H. F. Dos Santos, D. Paschoal, J. V. Burda, *Chem. Phys. Lett.* **2012**, *548*, 64–70.
[70] H. F. Dos Santos, D. Paschaol, J. V. Burda, *J. Phys. Chem. A.* **2012**, *116*, 11015–11024.
[71] H. F. Dos Santos, *Comput. Theor. Chem.* **2014**, *1048*, 95–101.
[72] H. F. Dos Santos, M. A. Vieira, G. Y. Sánchez Delgado, D. Paschoal, *J. Phys. Chem. A* **2016**, *120*, 2250–2259.
[73] G. Y. Sánchez Delgado, D. Paschoal, H. F. Dos Santos, *Comput. Theor. Chem.* **2017**, *1108*, 86–92.
[74] G. Y. S. Delgado, D. Paschoal, H. F. Dos Santos, *J. Biol. Inorg. Chem.* **2018**, *23*, 1283–1293.
[75] G. Y. S. Delgado, D. Paschoal, M. A. L. De Oliveira, H. F. Dos Santos, *J. Inorg. Biochem.* **2019**, *200*, 110804.
[76] J. M. Seminario, *Int. J. Quantum Chem. Quantum Chem. Symp.* **1996**, *30*, 1271–1277.
[77] S. Zheng, Q. Tang, J. He, S. Du, S. Xu, C. Wang, Y. Xu, F. Lin, *J. Chem. Inf. Model.* **2016**, *56*, 811–818.
[78] M. Frisch, G. W. Trucks, H. Schlegel, G. Scuseria, M. Robb, J. Cheeseman, G. Scalmani, V. Barone, B. Mennucci, G. A. Petersson, H. Nakatsuji, M. Caricato, X. Li, H. P. Hratchian, A. F. Izmaylov, J. Bloino, G. Zheng, J. L. Sonnerberg, M. Hada, M. Ehara, K. Toyota, R. Fukuda, J. Hasegawa, M. Ishida, T. Nakajima, Y. Honda, O. Kitao, H. Nakai, T. Vreven, J. A. Montgomery, J. E. Peralta, F. Ogliaro, M. Bearpark, J. J. Heyd, E. Brothers, K. N. Kudin, V. N. Staroverov, R. Kobayashi, J. Normand, K. Raghavachari, A. Rendell, J. C. Burant, S. S. Iyengar, J. Tomasi, M. Cossi, N. Rega, J. M. Millam, M. Klene, J. E. Knox, J. B. Cross, V. Bakken, C. Adamo, J. Jaramillo, R. Gomperts, R. E. Stratmann, O. Yazyev, A. J. Austin, R. Cammi, C. Pomelli, J. W. Ochterski, R. L. Martin, K. Morokuma, V. G. Zakrzewski, G. A. Voth, P. Salvador, J. J. Dannenberg, S. Dapprich, A. D. Daniels, Ö. Farkas, J. B. Foresman, J. V. Ortiz, J. Cioslowski, D. J. Fox, *Gaussian 09*; Gaussiann Inc.: Wallingford, CT, 2009.
[79] T. T. Tavares, G. C. Azevedo, A. Garcia, A. G. Carpanez, P. M. Lewer, D. Paschoal, B. L. Müller, H. F. Dos Santos, R. C. Matos, H. Silva, R. M. Grazul, A. P. S. Fontes, *Polyhedron* **2017**, 132, 95–104.
[80] M. L. Verdonk, J. C. Cole, M. J. Hartshorn, C. W. Murray, R. D. Taylor, *Proteins Struct. Funct. Genet.* **2003**, *52*, 609–623.
[81] O. Korb, T. Stu, T. E. Exner, *J. Chem. Inf. Model.* **2009**, 49, 84–96.
[82] H. R. Drew, R. M. Wing, T. Takano, C. Broka, S. Tanaka, K. Itakura, R. E. Dickerson, *Proc. Natl. Acad. Sci. USA* **1981**, *78*, 2179–2183.
[83] J. Wang, R. M. Wolf, J. W. Caldwell, P. A. Kollman, D. A. Case, *J. Comput. Chem.* **2004**, 25, 1157–1174.
[84] J. F. Lopes, V. S. A. Menezes, H. A. Duarte, W. R. Rocha, W. B. De Almeida, H. F. Dos Santos, *J. Phys. Chem. B.* **2006**, *110*, 12047–12054.
[85] D. A. Case, R. M. Betz, D. S. Cerutti, T. E. Cheatham III, T. A. Darden, R. E. Duke, T. J. Giese, H. Gohlke, A. W. Goetz, N. Homeyer, S. Izadi, P. Janowski, J. Kaus, A. Kovalenko, T. S. Lee, S. LeGrand, P. Li, C. Lin, T. Luchko, R. Luo, B. Madej, D. Mermelstein, K. M. Merz, G. Monard, H. T. Nguyen, I. Omelyan, A. Onufriev, D. R. Roe, A. Roitberg, C. Sagui, C. L. Simmerling, W. M. Botello-Smith, J. Swails, R. C. Walker, J. Wang, R. M.

Wolf, X. Wu, L. Xiao, P. A. Kollman, *AMBER 2016*, University of California, San Francisco, **2016**.
[86] J. A. Maier, C. Martinez, K. Kasavajhala, L. Wickstrom, K. E. Hauser, C. Simmerling, *J. Chem. Theory Comput.* **2015**, *11*, 3696–3713.
[87] M. Zgarbová, J. Šponer, M. Otyepka, T. E. Cheatham, R. Galindo-Murillo, P. Jurečka, *J. Chem. Theory Comput.* **2015**, *11*, 5723–5736.
[88] C. Rappel, M. Galanski, A. Yasemi, L. Habala, B. K. Keppler, *Electrophoresis* **2005**, *26*, 878–884.
[89] L. G. Danielsson, Y. H. Zhang, *TrAC Trends Anal. Chem.* **1996**, *15*, 188–196.
[90] M. Kah, C. D. Brown, *Chemosphere* **2008**, *72*, 1401–1408.
[91] I. H. J. Ploemen, M. Prudêncio, B. G. Douradinha, J. Ramesar, J. Fonager, G. J. Van Gemert, A. J. F. Luty, C. C. Hermsen, R. W. Sauerwein, F. G. Baptista, M. M. Mota, A. P. Waters, I. Que, C. W. G. M. Lowik, S. M. Khan, C. J. Janse, B. M. D. Franke-Fayard, *PLoS One* **2009**, *4*, 1–12.
[92] A. A. Sultan, V. Thathy, V. Nussenzweig, R. Ménard, *Infect. Immun.* **1999**, *67*, 2602–2606.
[93] Z. W. Chang, B. Malleret, B. Russell, L. Rénia, C. Claser, *Antimicrob. Agents Chemother.* **2016**, *60*, 6859–6866.
[94] M. Vanaerschot, L. Lucantoni, T. Li, J. M. Combrinck, A. Ruecker, T. R. S. Kumar, K. Rubiano, P. E. Ferreira, G. Siciliano, S. Gulati, P. P. Henrich, C. L. Ng, J. M. Murithi, V. C. Corey, S. Duffy, O. J. Lieberman, M. I. Veiga, R. E. Sinden, P. Alano, M. J. Delves, K. L. Sim, E. A. Winzeler, T. J. Egan, S. L. Hoffman, V. M. Avery, D. A. Fidock, *Nat. Microbiol.* **2017**, *2*, 1403–1414.

Manuscript received: August 25, 2020
Revised manuscript received: November 2, 2020
Version of record online: ■■, ■■■

FULL PAPERS

Three in one: A novel multitarget metallo-hybrid of chloroquine and primaquine linked by gold(I) with potent antiparasitic activity and selectivity against two different stages of malaria – the blood (asexual) and the liver stage – has been developed. It acts on at least three identified targets of the parasite: it inhibits the β-hematin formation, interacts with DNA and interacts of PfTrxR.

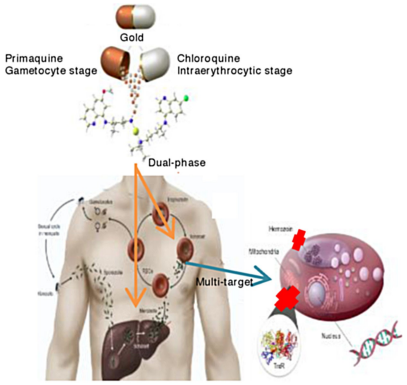

*C. de Souza Pereira, H. Costa Quadros, Dr. D. R. Magalhaes Moreira, Dr. W. Castro, R. I. Santos De Deus Da Silva, Dr. M. Botelho Pereira Soares, Dr. D. Fontinha, Dr. M. Prudêncio, V. Schmitz, Prof. H. F. Dos Santos, M. Gendrot, I. Fonta, J. Mosnier, Dr. B. Pradines, Prof. M. Navarro**

1 – 18

A Novel Hybrid of Chloroquine and Primaquine Linked by Gold(I): Multitarget and Multiphase Antiplasmodial Agent